MULTIPHASE FLOW MODELING AND ANALYSIS OF FILLING PROCESS FOR PULSED DETONATION ENGINES

by

SWATI CHANDRAN THIRUMANGALATH

Presented to the Faculty of the Graduate School of

The University of Texas at Arlington in Partial Fulfillment

of the Requirements

for the Degree of

MASTER OF SCIENCE IN AEROSPACE ENGINEERING

THE UNIVERSITY OF TEXAS AT ARLINGTON

MAY 2015

Acknowledgements

A handful people have influenced me academically and personally over the years that resulted in this thesis. This work is as much an attribute to them and their expertise as it is a projection of my academic achievement. As this may be the one time I could express my gratitude to these special people in writing, I would like to be more flamboyant than needed.

Dr. Frank K. Lu has been extremely supportive and gave me the liberty to pursue the research without restrictions. He encouraged me to not only grow as an independent researcher but also nurtured me to meet his high level of work expectations. I have been greatly fortunate to have a supervisor who thought such a great amount about my work, and who replied to my inquiries and questions so spontaneously.

I am obligated to my thesis committee members, Dr. Donald Wilson and Dr. Ankur Jain, for investing extra time and for their valuable comments about this work. I would like to acknowledge the Pointwise™ team for their generous assistance for conducting a free workshop which was very insightful on mesh generation techniques. I would like to thank David Carter for the technical support and timely license upgrades, and the Aerodynamics Research Center for their sense of support.

I dedicate this thesis to my grandmother who demonstrated to me the genuine worth of diligent work. Lastly, I thank my parents for permitting me to be as ambitious as I desired and for constantly reminding me about the bigger picture.

.

April 6, 2015

Abstract

MULTIPHASE FLOW MODELING AND ANALYSIS OF FILLING PROCESS FOR PULSED DETONATION ENGINES

Swati Chandran, M.S

The University of Texas at Arlington, 2015

Supervising Professor: Frank K. Lu

The filling process of a pulsed detonation engine with fuel and oxidizer should be carried out quickly in order to maintain a high frequency of operation. The objectives of this research were to model an efficient inlet system for filling the detonation tube with fuel/air mixture in stoichiometric ratio and to evaluate various filling schemes. Numerical modeling of the filling process was done using Pointwise™ for meshing and Fluent™ as the flow solver, solving the Reynolds-averaged Navier-Stokes equations with a k-ε turbulence model. Five different filling configurations were studied, including endwall, normal and angled, opposing and staggered sidewall. The fuel choices were biogas, hydrogen, methane, propane and octane all in the gaseous state. Oxidizer considered was air. The reactants were injected pre-mixed with an equivalence ratio of unity, at different velocities into a tube initially filled with ambient air at standard conditions. The benchmark was when the tube was 90 percent filled. It was found that staggered sidewall injection was the best configuration for rapidly filling the tube.

Table of Contents

List of Illustrations

List of Tables

Chapter 1

Introduction

Pulsed detonation engines (PDEs) have come under intense interest in the past two decades for their potential to revolutionize propulsion and power production [1],[2]. For propulsion applications, the fuel is detonated to produce thrust. The PDE has been shown to be theoretically more efficient than current engines based on the Brayton cycle. Moreover, there are some other potential advantages such as simplicity in design, manufacture and maintenance, as well as compactness [3].

In a PDE, a reactive gas mixture fills the combustion chamber and a detonation is then initiated. Thrust is generated by the high pressure and the momentum flux from the chamber. By repeating this cycle at high frequency, quasi-steady thrust levels can be generated.

Detonations

A strong shock wave compresses the reactants to produce a rapid, supersonic combustion. The coupled shock wave and supersonic combustion reaction is known as a detonation. Consider a detonation wave propagating in a tube filled with a combustible mixture. With one end of the tube closed and the other end open, the detonation is initiated near the closed end and propagates towards the open end. It is a strong shock that compresses the reactants which in turn initiates a combustion. This shock wave moves at the velocity of the detonation wave V_{det} relative to the gas in the chamber The thermodynamics of the process can be represented conveniently by a T–S diagram as shown in Figure 1-1.

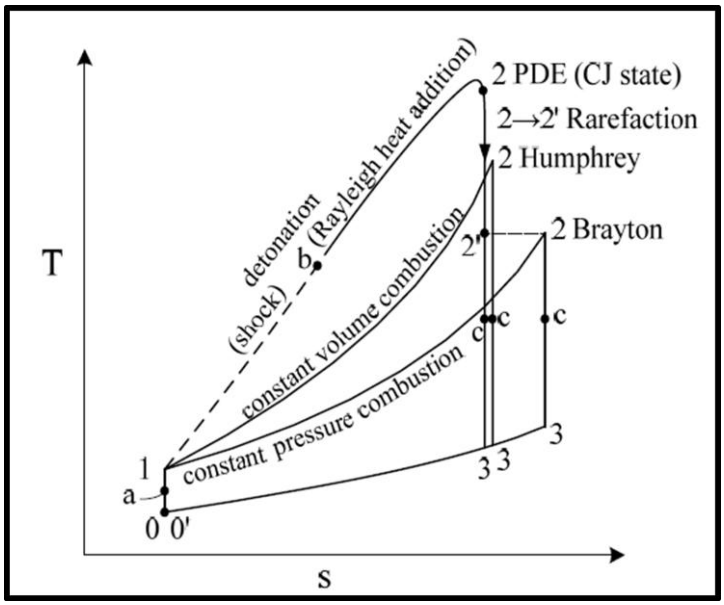

Figure 1-1 T-S diagram for ideal cycles: a detonation cycle compared to a Humphrey (isochoric combustion) and a Brayton (isobaric combustion) cycle [3]

Figure 1-1 shows a "pre-compression" from 0 to 1 as a necessary stage for the Brayton cycle but not needed for the Humphrey or the detonation cycle, sometimes called the Zel'dovich-von Neumann-Döring (ZND) cycle for short. The pre-compression is strictly not needed for the Humphrey or ZND cycle since the compression arises from the shock. Focusing attention to the ZND cycle, the figure shows that the temperature and the pressure in the working gas are both increased drastically from T_1 to T_b and P_1 to P_b. The high pressure peak is known as the von Neumann spike. The high temperature initiates chemical reactions. The chemical kinetics of the gas mixture influences the width of this region which represents the ignition delay.

The temperature is increased as heat is added through a supersonic Rayleigh process from the exothermic chemical reactions and thereby the pressure is decreased. The time taken to complete the combustion reaction determines the width of the heat

addition region. The gas is completely burned at state 2, which is Chapman-Jouguet (CJ) condition for a self-sustaining detonation. At state 2, the temperature, pressure and density of the gas are greater than at state 1 and the gas is in thermodynamic equilibrium. The CJ temperature T_2 is higher than the von Neumann spike due to heating. In the case of a detonation propagating from a closed end of a tube, an unsteady expansion known as the Taylor rarefaction develops behind the heat addition region. Rarefaction waves are generated from the closed end that keep the normal velocity of the gas at the wall at zero. The expansion results in a pressure drop in the burned gas in the detonation tube [6].

Thermodynamics of Deflagration and Detonation Cycles

A detonation engine has for a long time been conceptualized as a constant volume process, known as the Humphrey cycle. It is important to note that the detonation is actually not a constant volume process. Figure 1-1 also shows the difference between the Humphrey cycle, the correct ZND cycle and, for comparison, the Brayton cycle as representing a conventional gas generator. In the figure, there is the same amount of compression from 0→1 for all three cycles although in practice these should either not be needed or should be smaller for the Humphrey and ZND cycles. Qualitatively, the ZND cycle has higher work output and efficiency than the Humphrey and Brayton cycles, with Brayton cycle having the lowest [3].

PDE Gasdynamics Processes

As the name suggests, the engine operates in a pulsed or cyclical manner. A schematic of the different stages of a cycle is shown in Figure 1- 2. For the present discussion, the cycle starts with the tube also known as a chamber that is initially at

ambient conditions, as shown in the top of Figure 1- 2. Going clockwise in the figure, the tube is filled with premixed reactants, shown schematically to be from the closed end. The reactants propagate to the right, completing the filling in a time of t_{fill}. Next, a detonation wave is initiated, which takes a time of t_{init} to complete. The detonation wave propagates through the tube, taking a time of t_{det} to do so. The exit of the detonation wave induces an unsteady expansion to propagate into the chamber. This may be followed by a purging process in order to prevent auto ignition of the incoming reactants for the next cycle.

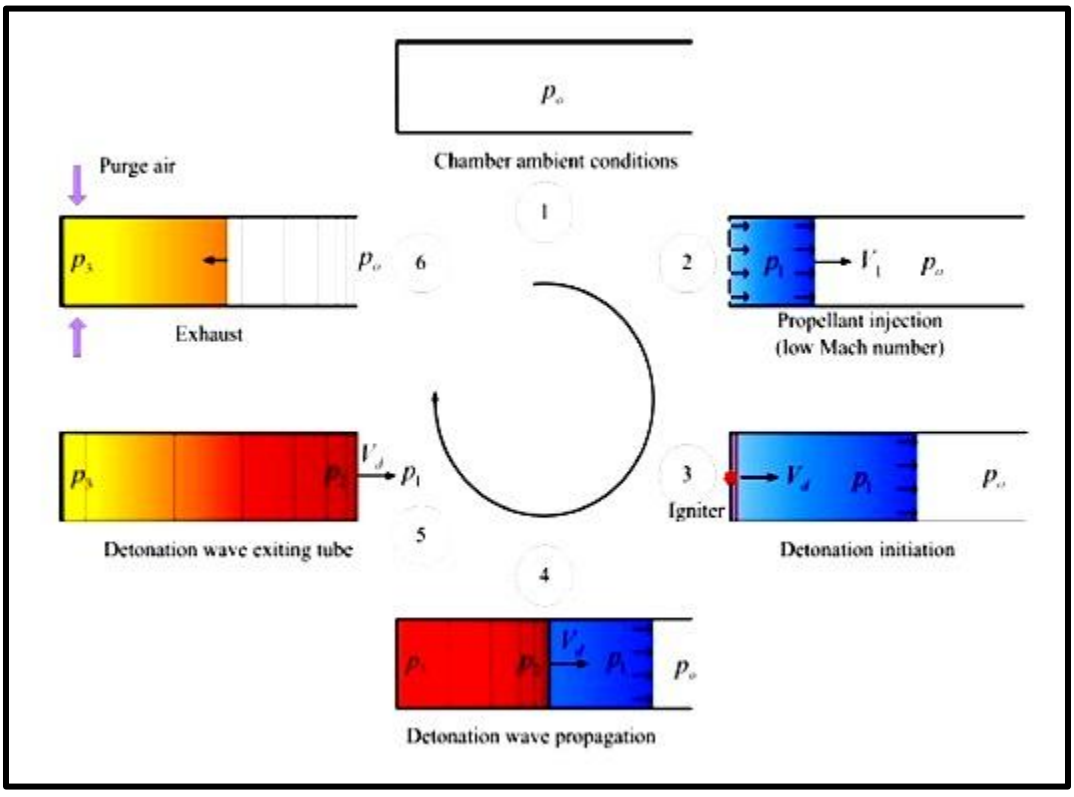

Figure 1- 2 Key stages of a PDE cycle [3]

Filling Process

The PDE detonation process happens in a tube with one open and one closed end, with the detonation initiating at or near the closed end. The entire detonation cycle starts with an empty tube, in which a fuel/oxidizer mixture is filled through a valve at the closed end. Step 2 of the Figure 1- 2 shows the filling process [7]. The fill time is calculated as

$$t_{fill} = \frac{\text{Length of the tube}}{\text{Filling velocity}} = \frac{x_l}{V_{fill}} \tag{1.2}$$

Detonation Process

Once the filling process is complete, the fuel and oxidizer valves are closed while the combustor exit remains open. A deflagration is initiated at the closed end of the chamber using an ignition source. This deflagration quickly transitions into detonation.

The detonation wave propagates inside the tube and the combusted gases are then exhausted. In order to prevent any unburnt pockets of gases, the detonation wave and the propellant mixture reach the combustor exit at the same time and this process is determined by valve timing. An unsteady rarefaction zone is created between the detonation wave and the closed end in order to keep the velocity at zero at the closed end. Steps 3 and 4 of Figure 1- 2 depict the initiation and detonation processes respectively. The detonation time is given by

$$t_c = \frac{\text{Length of the tube}}{\text{CJ wave velocity}} = \frac{x_L}{D_{CJ}} \tag{1.2}$$

Due to the speed of the detonation wave being so much faster than the propagating reactant front or the subsequent blowdown and purge processes, this phase is the fastest one and is frequently neglected in computing the cycle time or the inverse, operating frequency of the PDE.

Blowdown Process

The detonation wave exits the chamber through the open end. At this stage, the chamber will contain combustion products at high temperature and pressure. The axial velocity of these products varies from zero at the closed end to supersonic values at the exit.. As the wave exits the chamber, a pressure differential is created at the open end which generates a series of rarefaction waves that are locally sonic. This unsteady rarefaction creates an unsteady blowdown process and is reflected off the closed end as expansion waves. These unsteady rarefaction and expansion waves are generated and reflected alternately. They accelerate the burned gases towards the exit. The time taken for the blowdown stage is given by [7]

$$t_b = \frac{\text{Length of the tube}}{\text{Rarefaction velocity}} = \frac{4x_L}{D_{CJ}} \tag{1.3}$$

Purge Process

Finally, as has been shown to be a necessity in numerous studies, a purge process pumps cold air into the detonation tube to scavenge it from combustion products and also to help cool it. The time required to purge the tube is approximately the same as t_{fill} and is given by

$$t_{purge} = \frac{\text{Length of the tube}}{\text{Purging velocity}} = \frac{x_L}{V_{purge}} \tag{1.4}$$

There can be variations from the process described above. For example, it may not be necessary to wait until the reactants to reach the end of the tube to ignite the mixture. Similarly, the purge process can start before the detonation wave exits the tube. There is also the possibility of sidewall injection to speed up the fill process and to improve the fill fraction.

Since the energy for direct initiation of detonation is exorbitantly high, it is usual to rely on a deflagration-to-detonation transition (DDT) process. In this process, a lower energy source is used to ignite the propellants. A deflagration wave propagates in the tube and transitions to a detonation process. This natural DDT process is actually quite long which is detrimental for PDEs, resulting in a bulky and heavy device. In addition, the time taken to develop the detonation is long which means a lower operational frequency. Therefore, in practice, DDT devices such as Shchelkin spirals or orifice plates are inserted near the igniter to promote early onset of detonation. Most of the PDEs reported in the literature have long detonation tubes to satisfy the deflagration-to-detonation transition requirement [4], even with transition enhancement devices such as the aforementioned ones. For mixtures of air and hydrogen or gaseous hydrocarbons, a tube of 1 m length and 100 mm diameter appears to be adequate for satisfying the DDT length and detonation cell width requirements. Smaller dimensions such as a length of 0.1 m and a diameter of 50 mm are generally adequate for gaseous fuel and oxygen mixtures. The larger diameter requirement for air is because of the need to accommodate the large detonation cell sizes [5]. Both the length and the volume of such detonation tubes make it difficult to have a short fill or purge time due to the need to fill a large volume and the slow speed of the propellant front if the tube is filled from one end.

From the above discussion, the cycle time comprises of the filling, initiation, detonation wave propagation and purging times:

$$t_{cyc}=t_{fill}+t_{init}+t_{det}+t_{purge} \tag{1.5}$$

System studies suggest that PDEs for aerospace applications should operate at frequencies of 50–100 Hz, so that the cycle time is 10–20 ms. Of the components that make up the cycle time in Eq. (1.5), the fill and purge times are the longest due to the relative slowness of filling the tube with reactants or cold air respectively. For example, for filling from the closed wall at a speed of 40 m/s, a 1 m tube will be filled in 25 ms which is way longer than the above-quoted range of cycle times.

High fill rates may be desirable but this incurs large pumping requirements, adding to complexity, volume and weight. The simple estimate above shows conflicting requirements between rapid fill (and purge) and a reasonable DDT length for reliable detonations, as well as the need to fill a large volume to ensure consistent, cycle-to-cycle performance. Additionally, the inlet configurations may result in “dead air” regions that can diminish the PDE performance, such as erratic detonation. In view of the conflicting requirements mentioned above, a numerical study was performed on alternative fill strategies. An advantage of a numerical study is that details of the filling process can be revealed and evaluated.

The overall concept is that if extra ports are available for sidewall filling, then the tube can be filled more rapidly. Different sidewall filling configurations were studied and the most promising configuration was selected. The next stage of the study was to increase the fill rate for the most promising configuration. Moreover, different stoichiometric fuel–air mixtures at STP were used to fill the tube.

Chapter 2

Methodology

Multiphase Flows

The presence of more than one material in different or the same physical states of matter gives way to a multiphase flow field. The different materials in a multiphase flow field can be represented as primary and secondary phases. The problem statement here makes use of a gas-gas interface for the gaseous fuels and air. The continuous phase is air and is also called the primary phase. The gaseous fuel is the distributed material and is known as the secondary phase. Multiphase flow regimes can be laminar or turbulent in the same channel. Some common flow regimes can be seen in Table 2-1 below.

Table 2-1 Summary of multiphase flow regimes

Flow Regime Type	**Primary Phase/Secondary Phase**
Bubble/slug flow	Liquid/discrete bubbles of gas
Droplet/dispersed/spray flow	Gas/droplets of fluid (liquid or gas)
Particle-laden flow	Fluid (liquid or gas)/discrete particles of solid
Slug flow	Liquid/large bubbles of gas
Annular flow	Liquid along walls with gaseous flow core
Stratified/wavy and free-surface flow	Immiscible fluids; less dense fluid flows atop dense fluid with definitive interface between fluids

The center node FVM (finite volume method) discretization technique using both segregated and coupled solution methods can be implemented with the Fluent™ solver.

The Euler–Euler multiphase models available were the Eulerian, mixture, VOF (volume of fluid) and discrete phase. Eulerian and mixture models are used for bubbly, droplet or particle laden flows in which the phases mix and the dispersed phase volume fraction exceeds 10%. The VOF model can be applied for free surface flows having distinct/separate phases with an interface between them. This model employs a surface tracking technique which was more applicable for capturing dead air regions when applied to a fixed Eulerian mesh.

Navier-Stokes Equation and Turbulence Model

The fluid flow can be solved numerically by a RANS (Reynolds-averaged Navier–Stokes) solver with a realizable *k*-ε turbulence model. A single phase flow can be modeled using the continuity and momentum equations (collectively known as the Navier–Stokes equations). These will continue to be the basis for multiphase flows. The only difference is in the capturing the interface which determines the exchange between the two phases. The continuity and momentum equations are written as

$$\frac{\partial \rho}{\partial t} + \nabla(\rho u) = 0 \tag{2.1}$$

$$\frac{\partial \rho u}{\partial t} + \nabla(\rho u u) = -\nabla p + \nabla \tau \tag{2.2}$$

where ρ is the density, u is the instantaneous velocity, p is the pressure, τ is the viscous stress tensor and gravity has been ignored.

The realizable k–ε model can be defined by the following two transport equations: the first is for the turbulent kinetic energy k and second for the rate of dissipation of turbulent kinetic energy ε

$$\frac{\delta}{\delta t}(\rho\kappa) + \frac{\delta}{\delta x_j}(\rho\kappa u_j) = \frac{\delta}{\delta x_j}\left[\left(\mu + \frac{\mu_t}{\sigma_\kappa}\right)\frac{\delta\kappa}{\delta x_j}\right] + G_\kappa + G_b - \rho\varepsilon - Y_M + S_\kappa \tag{2.3}$$

$$\frac{\delta}{\delta t}(\rho\varepsilon)+\frac{\delta}{\delta x_j}(\rho\varepsilon u_j)=\frac{\delta}{\delta x_j}\left[\left(\mu+\frac{\mu_t}{\sigma_\varepsilon}\right)\frac{\delta\varepsilon}{\delta x_j}\right]+\rho C_1 S_\varepsilon-\rho C_2\frac{\varepsilon^2}{\kappa+\sqrt{\nu\varepsilon}}+C_{1\varepsilon}\frac{\varepsilon}{\kappa}C_{3\varepsilon}G_b+S_\varepsilon \quad (2.4)$$

where G_κ represents the turbulence kinetic energy generated due to the mean velocity gradients, G_b represents the turbulence kinetic energy generated due to buoyancy, Y_M represents the contribution of the fluctuating dilatation in compressible turbulence to the overall dissipation rate, $C_{1\varepsilon}, C_{2\varepsilon}, C_{3\varepsilon}$ are constants, σ_κ and σ_ε are the turbulent Prandtl numbers and are defined as model constants with values of 1 and 1.2 respectively and S_κ and S_ε are source terms A wide range of flows, including rotating homogeneous shear flows, free flows and separated flows exploit this model and it has very well been validated. The performance of this model is better than the standard k-ε model [11].

Volume of Fluid Approach

Surface fitting and surface capturing are the two main approaches for maintaining a distinct interface in a simulation. The surface capturing approach implemented by Fluent™ makes use of the VOF scheme for modeling general multiphase flow fields. The volume fraction for each of the fluids was defined first. With the average fluid flow, the amount of convection of volume fraction for each fluid was computed. Near the vicinity of the interface, the volume fraction for each of the fluids was used to reconstruct the interface between the two fluids.

The volume of fluid model with the Euler–Euler approach is suitable for the present study because it can track sharp interfaces between two or more phases [11]. Both the reactant and the air phases were treated as separate, continuous phases with one set of governing equations solved for each. All field variables were assumed to be shared between the phases and the Navier–Stokes equations were modified to account

for the combined mixture properties. The criterion for the fill time was when the tube is filled 90 % with reactants.

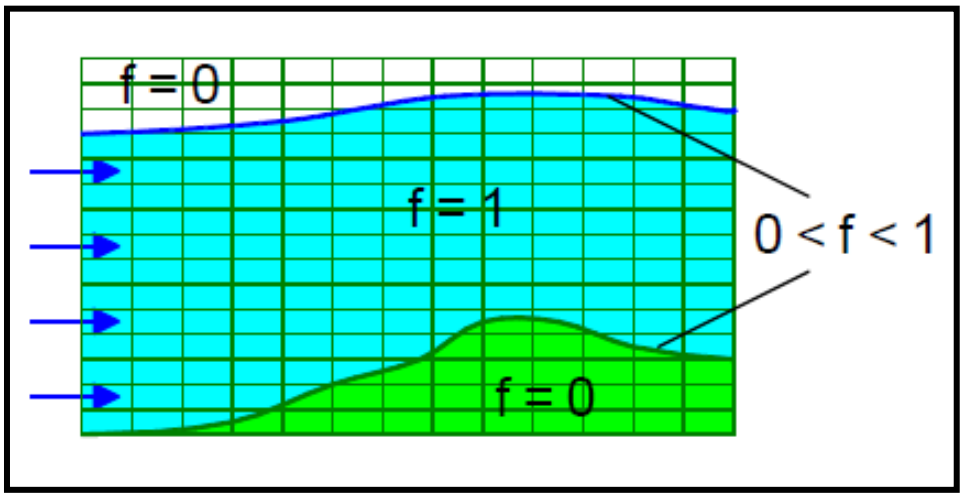

Figure 2-1 Interface tracking for VOF approach

The VOF approach uses a phase indicator function ∝, also known as a color function, in order to track the interface between two or more phases where

$\alpha_k=0$	Cell empty of the kth fluid
$\alpha_k=1$	Cell full of the kth fluid
$0<\alpha_k<1$	Cell contains interface between the kth fluid and one or more other fluids

When the control volume is entirely filled with one of the phases, the indicator value is one or zero. The indicator value is between zero and one if an interface exists in the control volume, thus demonstrating properties of volume fraction. Equations (2.1) and (2.2) are therefore modified for the VOF method to account for the two phases and all the field variables are shared between the phases, so that

$$\frac{d\rho_m}{dt}+\nabla(\rho_m u)=0 \tag{2.5}$$

$$\frac{d\rho_m u}{dt}+\nabla(\rho_m uu)=-\Delta P+\Delta\tau+S \tag{2.6}$$

$$\frac{d\alpha_k}{dt} + \nabla(\alpha_k u) = 0 \tag{2.7}$$

$$\rho_m = \sum \alpha_k \rho_k \tag{2.8}$$

where u is the instantaneous velocity, ρ is density, α is the volume fraction, P is the average pressure which is shared between phases, τ is the shear stress tensor, S represents the source term which is usually zero or it could be a mass source for each phase defined by the user, k is one of the phases and m is for the combined mixture properties. Equation (2.7) monitors the volume fraction of one (or more) of the phases used for tracking the interface between the phases. The entire domain was solved for the single momentum equation (Equation 2.6). A single set of the above transport equations was solved for the case of turbulence quantities. In the entire flowfield, the variables of k and ε were shared by the phases.

Equation (2.5) helps track the interface between two or more phases. The discretization of the phase indicator α is very important in order to obtain a sharp interface [14]. Implicit discretization scheme was used which makes use of the volume fraction at the current time step. Equation 2.9 was solved iteratively at each time step for the volume fraction of each of the secondary phases.

$$\frac{\alpha_2^{n+1}\rho_2^{n+1} - \alpha_2^n \rho_2^n}{\Delta t} V + \sum_f \left(\rho_2^{n+1} U_f^{n+1} \alpha_{2,f}^{n+1}\right) = 0 \tag{2.9}$$

Where $\alpha_{2,f}^{n+1}$ is the face value of the 2nd volume fraction,

and U_f^{n+1} is the volume flux through the face, based on normal velocity

Wilke's Formula

The present study considered stoichiometric gaseous mixtures of air with

a. Biogas
b. Methane

c. Propane

d. Octane

e. Hydrogen

Biogas was studied first since it provided greater advantages in power production with reduced emission [16]. The composition for Biogas is stated in Appendix B. In order to compute the viscosity of multicomponent gas mixtures, the Wilke's formula was used.

$$\mu_{mix} = \sum_{i=1}^{n} \frac{X_i \mu_i}{\sum_{j=1}^{n} X_j \phi_{ij}} \tag{2.10}$$

$$\phi_{ij} = \frac{1}{\sqrt{8}} \left(1 + \frac{M_i}{M_j}\right)^{-\frac{1}{2}} \left(1 + \left(\frac{\mu_i}{\mu_j}\right)^{\frac{1}{2}} \left(\frac{M_j}{M_i}\right)^{\frac{1}{4}}\right)^2 \tag{2.11}$$

where n is the total number of chemical species, X_i and X_j are mole fractions for the two species, μ_i and μ_j are viscosities of two species in kg/m/s, M_i and M_j are the molecular weight for the two species in kg/mol. The combined mixture properties were set up as premixed fuel for computations.

Segregated and Coupled Solvers

The pressure and velocity are strongly coupled in the discretized form of the governing equations. Segregated solvers and coupled solvers are available in Fluent™ for handling pressure-velocity coupling. The momentum equation contains pressure gradients and therefore the distribution of pressure needs to be accounted for. Knowing the pressure terms, the velocities could then be solved. A pressure correction equation was used by the segregated solver. The guessed values for pressure were used for solving the momentum equations. If the continuity equation was not satisfied by the resultant velocities, the solution was updated using the pressure correction equation.

Figure 2-2 shows the process flow for the segregated solver. The segregated solver versions available with Fluent™ are SIMPLE (Semi Implicit Method for Pressure Linked Equations), SIMPLEC (SIMPLE Consistent) and PISO (Pressure Implicit with Splitting of Operators). SIMPLEC and PISO are improved versions of SIMPLE because they permit the use of higher under relaxation factors. An equation for a certain variable was solved for all cells with segregated methods followed by the equation for the next variable again solved for all cells in the flow field. Cases 1, 4 and 5 used the SIMPLE algorithm. Memory requirements are low since only one discrete equation was stored. However, the rate of convergence is slower because of the iterative nature of the solution algorithm.

Figure 2-3 shows the process flow for coupled solvers. The momentum and continuity equations were solved simultaneously in a coupled solver. This approach was used in cases 2 and 3. The storage requirements were larger since the complete set of discrete equations was needed to be stored at the same time. Also, the coupled solver took considerably more amount of time to complete one iteration loop. However, convergence was achieved in relatively fewer iterations [12].

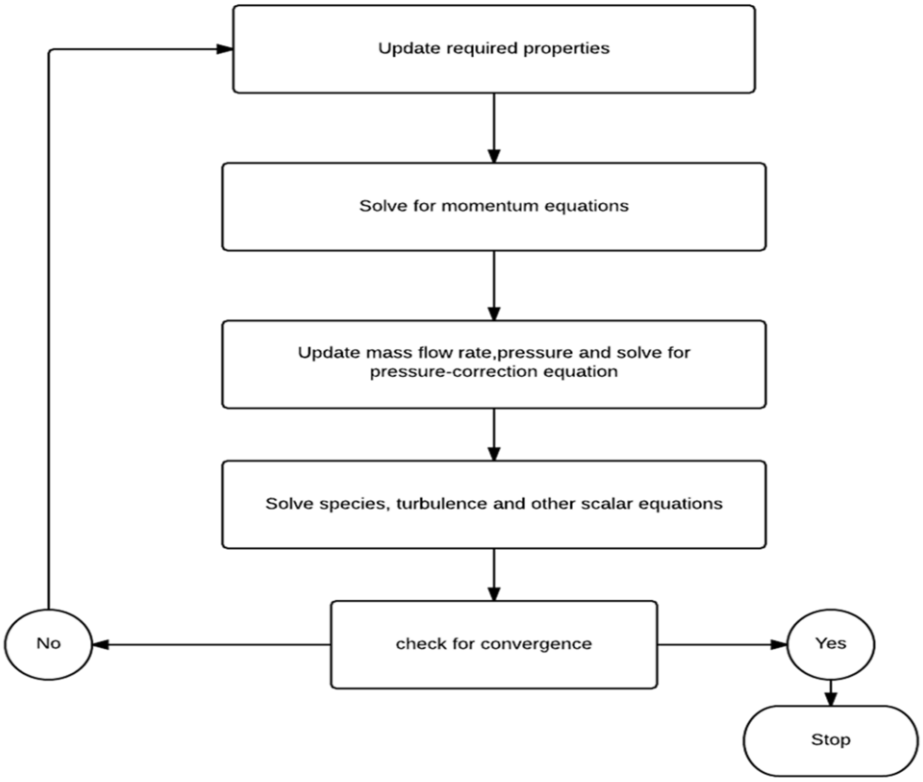

Figure 2-2 Segregated solver process schematic

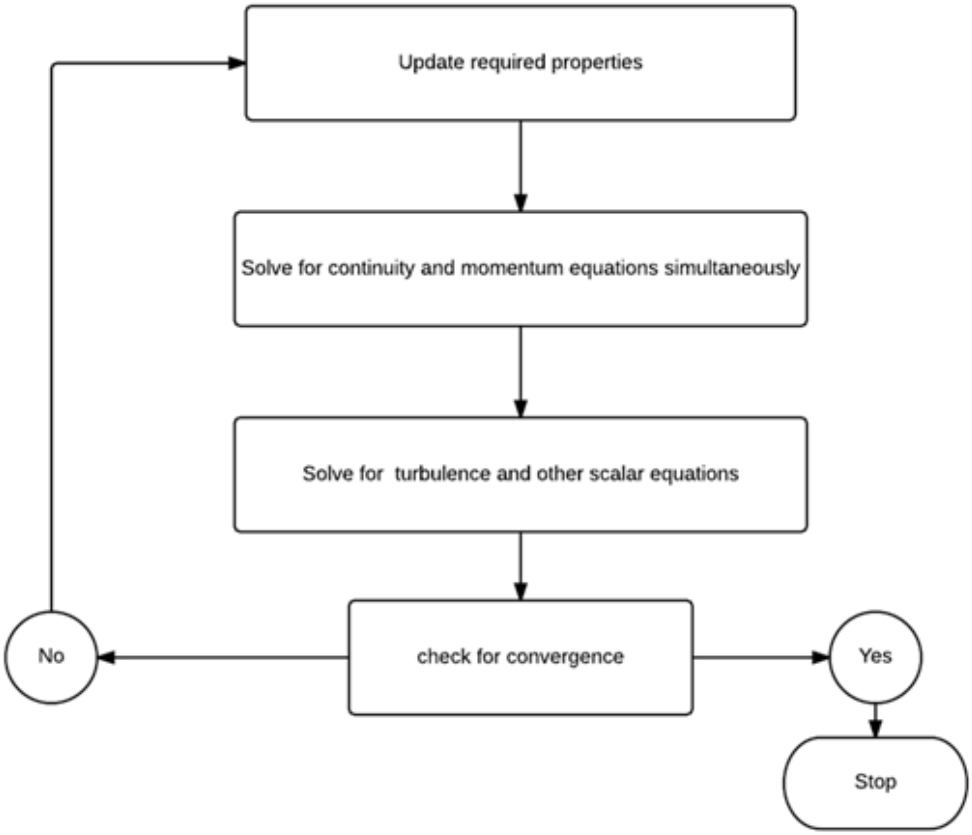

Figure 2-3 Coupled Solver Process Schematic

The methodology adopted consists of the following stages: pre-processing, solving for the flow variables and post-processing. The pre-processing stage involves geometry creation and mesh generation which were done using Pointwise™. Multiphase flows were modeled using the Fluent™ solver and the flow was visualized with CFD Post™. Figure 2-4 shows the CFD process flowchart which will be discussed in the sections below.

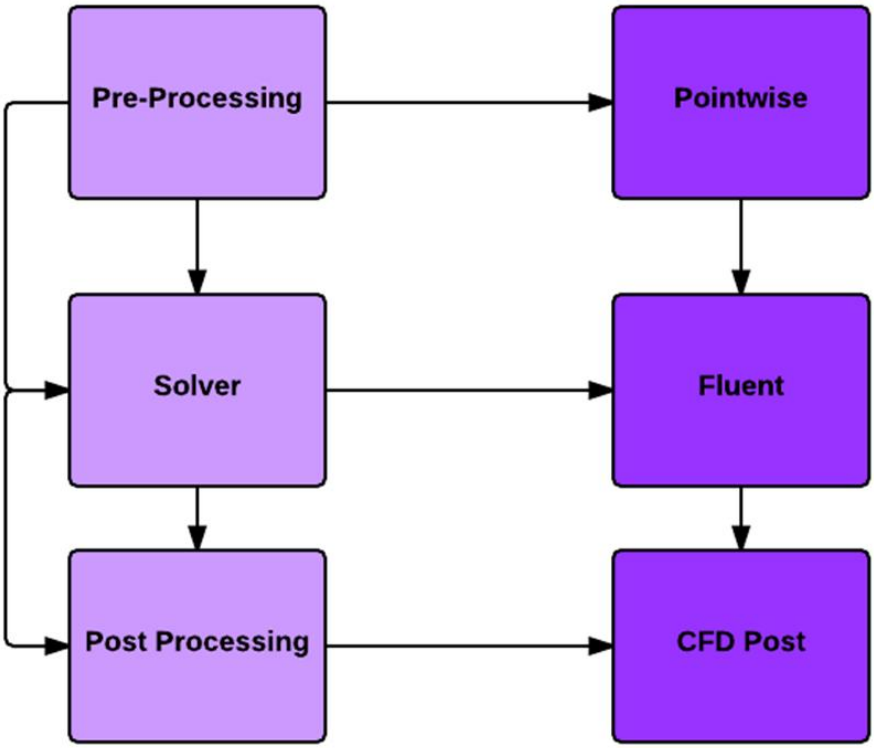

Figure 2-4 CFD Process Flowchart

Pre-processing

Geometry creation and mesh generation

A 1 m long detonation tube with 100 mm internal diameter was considered in this study. Only half of the PDE was modeled for computing efficiency and the symmetry condition was used [14].

A fully structured mesh was created for case 1 with an incoming average velocity of 180 m/s. A more refined hybrid mesh was generated for the other case studies. A sufficiently resolved surface mesh was first generated in order to capture the flow features. Both trimmed and untrimmed approaches were used [8]. The trimmed approach was used for case 3 and untrimmed approach for case 2. Owing to the ease of

generating grid cells, the untrimmed approach was employed for the rest of the cases. For the trimmed approach, the grid points were placed only on the exposed surfaces. The curve where the inlet topology intersects with the main body of the detonation tube and the symmetry plane curve were identified as surface features. In the untrimmed approach, the angle and orientation of the inlet geometry was maintained using a path extrusion technique. The resulting mesh consisted of multi-block grid elements.

Table 2-2 Mesh Specifications

Case	Tetrahedral cells	Pyramid cells	Prism Cells	Total Cells	Total Points
1	0	0	23,404	23,404	13,262
2	126,087	4,400	0	130,487	27,544
3	380,897	0	15,240	396,137	86,748
4	119,187	4,400	0	123,587	26,333
5	123,169	0	5,964	129,133	31,244

The untrimmed approach provided more flexibility for surface mesh generation and inlet creation. A higher resolution was achieved for the boundary layer and the reactant flow by making use of denser grid lines near the inlets and at the walls. The main inlet consists of prism cells, side inlets makes use of pyramid cells and the rest of the PDE was filled with tetrahedral cells. The mesh specifications for all the initial cases are shown in Table 2-2.

The structured domains were initialized using the standard, arc-length based trans-finite interpolation (TFI) scheme. As a result, grid lines were inside the domain boundaries. Maximum smoothing was achieved at the expense of clustering by solving for Laplace interior control functions. These control functions set the RHS values for the elliptic partial differential equations to zero in order to attain maximum smoothness. Ten

iterations were solved for keeping the surface shape fixed. The multi-grid solution algorithm was set to accelerate the smoothing procedure with a standard growth rate of 1.2 for initializing unstructured blocks and domains [9].

Case 1: Single end-wall injection

The geometry was made using a single end-wall injection port with a 20 mm inlet diameter as a baseline configuration as shown schematically in Figure 2-5. The figure shows a short 25 mm inlet for design purposes to simulate an actual PDE configuration although it does not actually affect the simulation. The results converged faster using a structured mesh along the length of the tube instead of an unstructured mesh, the grid being aligned with the flow direction. The propagation of reactants entering the detonation tube was captured more accurately by adopting a denser mesh near the inlet walls. The difference between the shape of an equilateral cell and the shape of a cell of equivalent volume is the skewness angle. The skewness angle of the cells was increased to 45^{o} at the exterior of the main body using a H-type topology alone. Modification to the grid topology was carried out later by creating an O-H or butterfly grid in Pointwise™.

O-type meshes were generated along the outer curved domain followed by H-type meshes in the interior for the front surface as shown in Figure 2-6(b). This removed the highly skewed cells created by the H-type mesh alone [10]. Steger-Sorenson boundary control ensured a more relaxed enforcement of spacing and angle between the grid lines, resulting in an overall smoother grid.

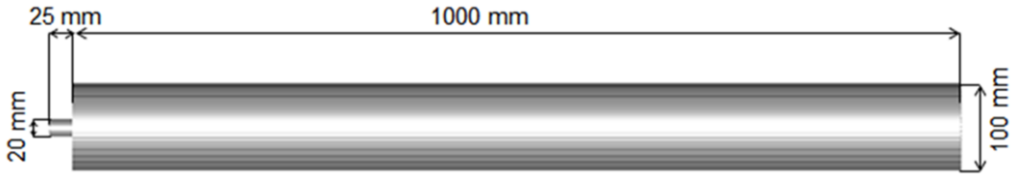

Figure 2-5 Case 1 geometry

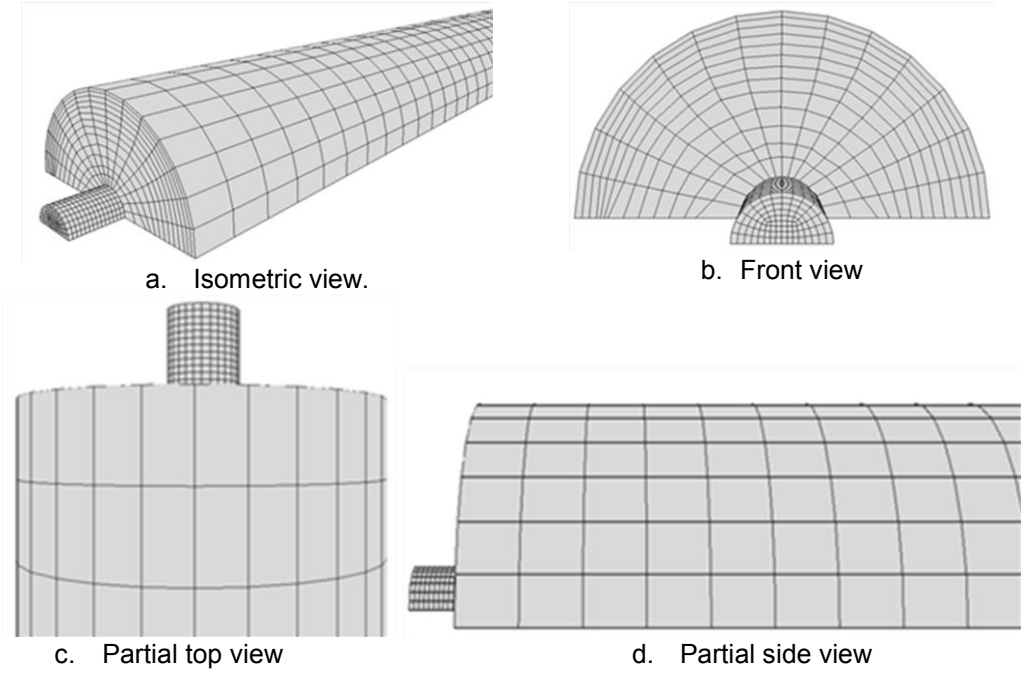

Figure 2-6 Case 1- different views of grid blocks

Case 2: Single end-wall injection with four opposite side-ports

Four pairs of side-ports were introduced on both sides of the detonation tube to speed up the fill time and to ensure efficient filling in an attempt to reduce void regions along the flow path. These side-ports were placed at 175, 375, 575 and 775 mm from the end-wall

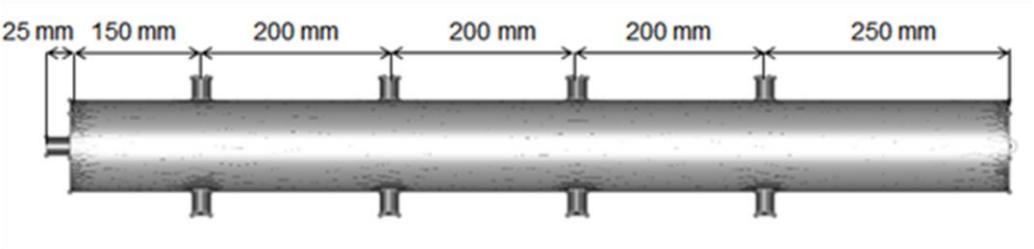

Figure 2-7 Case 2 geometry

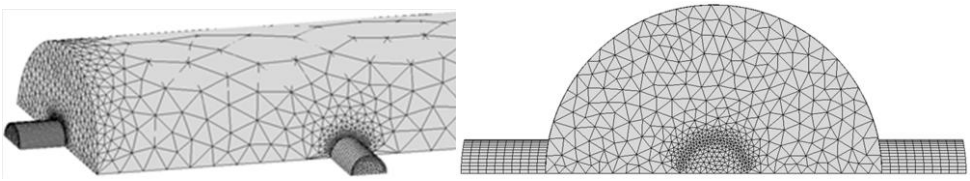

a. Isometric view b. Front view

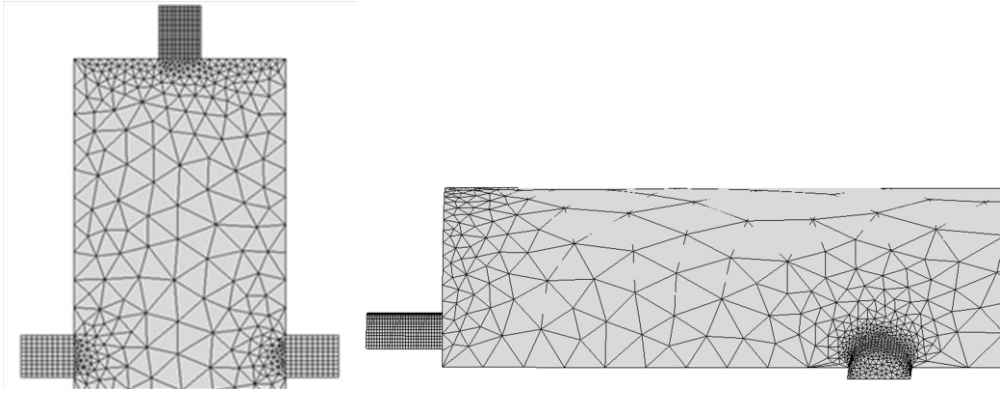

c. Partial side view d. Partial top view

Figure 2-8 Case 2- different views of grid blocks

inlet. All of these inlets had internal diameters of 20 mm similar to case 1 as can be seen in Figure 2-7. A structured grid was adopted along the inlets where the grid is flow aligned for varying velocity conditions. Eight prism layers were extruded at the filling inlet. These cells formed part of a separate fluid volume, which was patched during

initialization with a volume fraction of unity (i.e., these cells are filled with filling fluid). This was considered as a best practice for VOF modeling. The rest of the mesh was unstructured. The resulting mesh consisted of multi-block grid elements [17].

Case 3: Single end-wall injection with four opposite side-ports inclined upstream to the flow

This was similar to case 2 except the inlets were inclined upstream at 45^{o} to improve the fill fraction compared case 2 as shown in

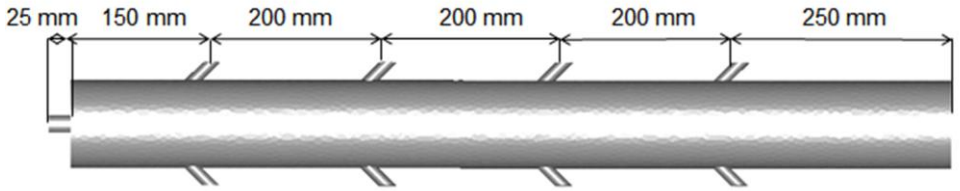

Figure 2-9 Case 3 geometry

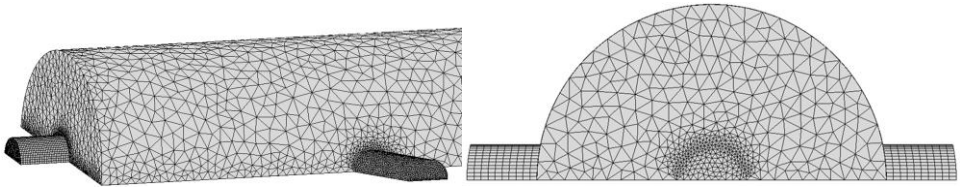

a. Front view b. Isometric view

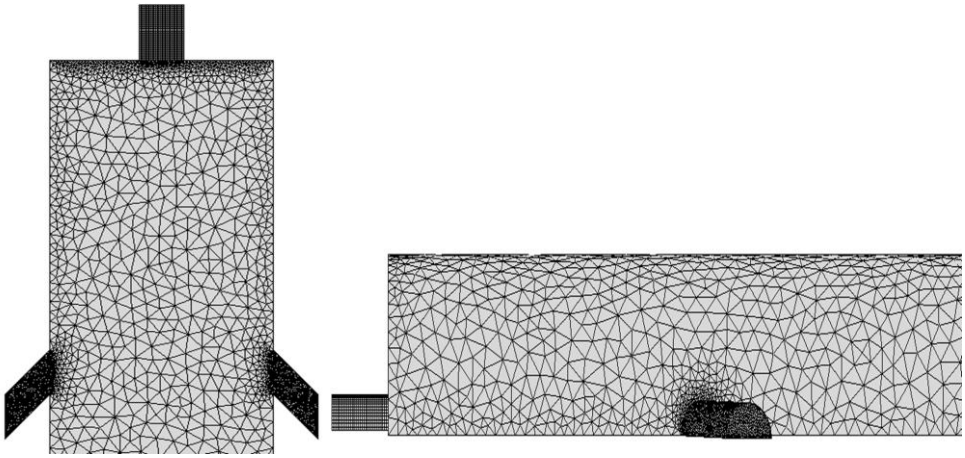

c. Partial top view d. Partial side view

Figure 2-10 Case 3- different views of grid blocks

Case 4: Single end-wall injection with four opposite side-ports inclined downstream to the flow

This was similar to case 3 except the inlets were inclined downstream as shown in Figure 2-11. It was thought that this configuration might help to speed up the filling process.

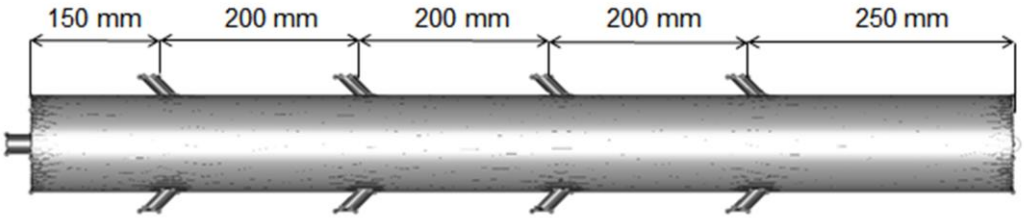

Figure 2-11 Case 4 geometry

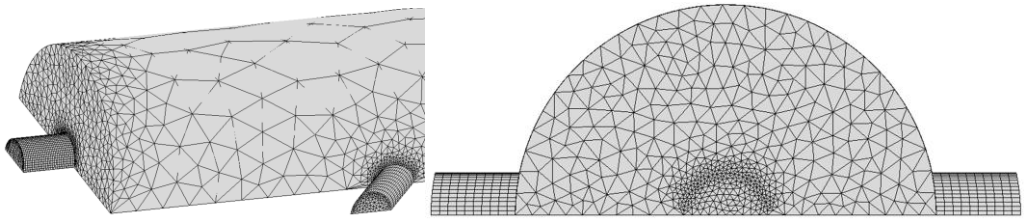

a. Isometric view b. Front view

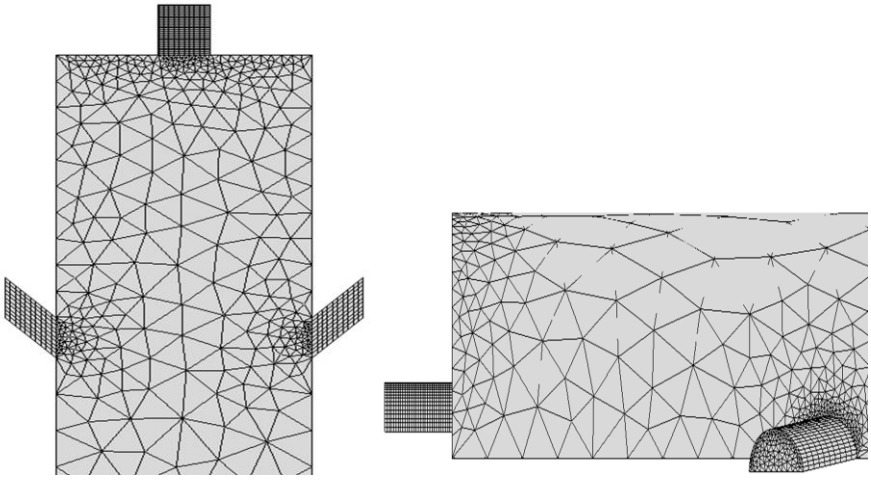

c. Partial top view d. Partial side view

Figure 2-12 Case 4- different views of grid blocks

Case 5: Single end-wall injection with four opposite side-ports inclined upstream to the flow

The inlets were equally spaced and inclined upstream at 45^{o} to improve the fill fraction as well as to reduce isolated pockets of gas.

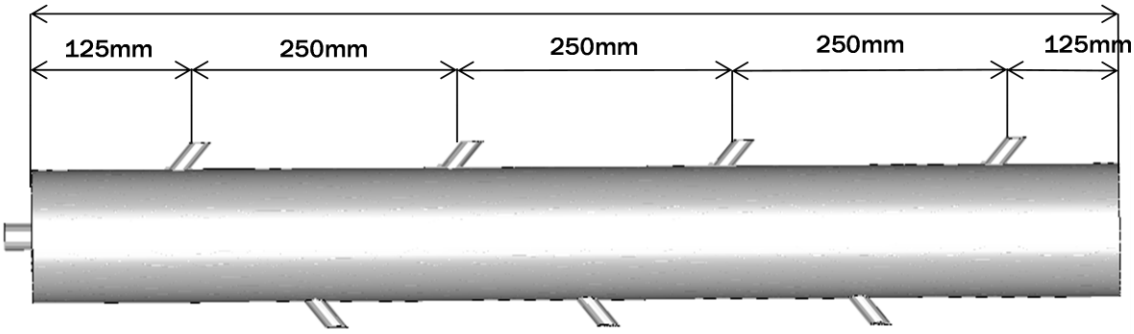

Figure 2-13 Case 5 geometry

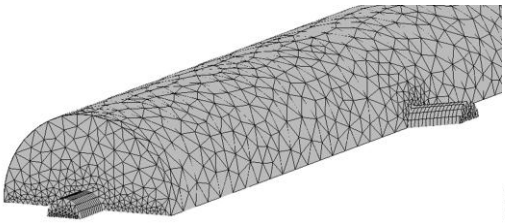

e. Isometric view

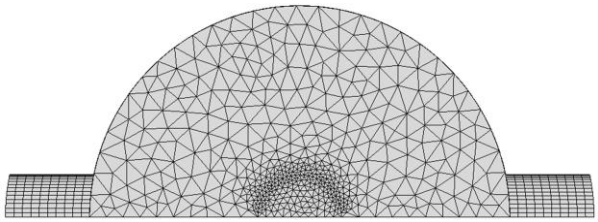

f. Front view

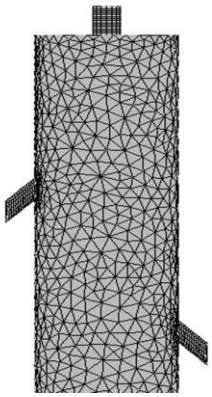

g. Partial top view

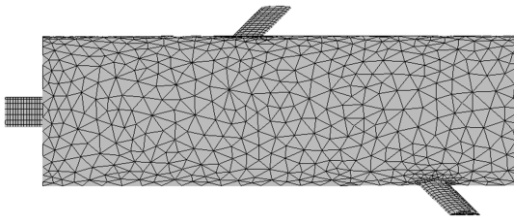

h. Partial side view

Figure 2-14 Case 5- different views of grid blocks

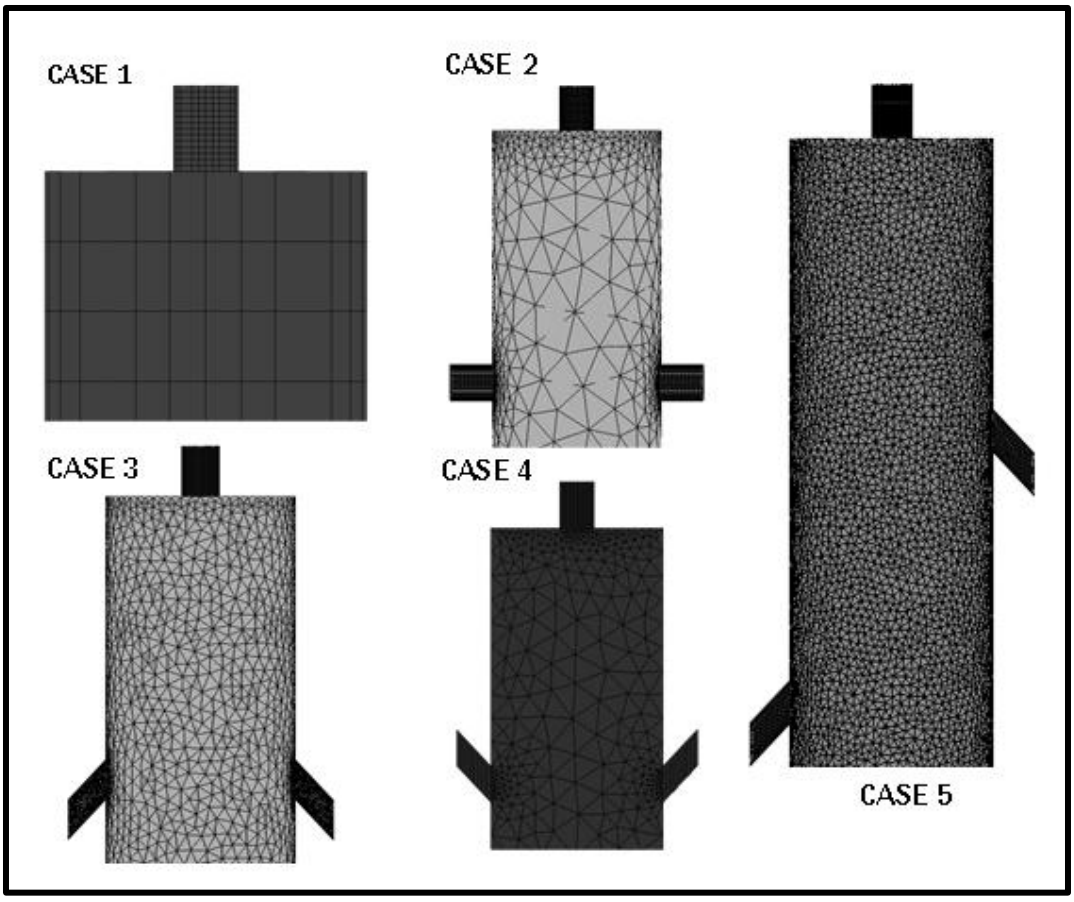

Figure 2-15 Summary of all five cases

Figure 2-15 shows the summary of all the 5 cases/designs, namely, endwall, normal , angled, opposing and staggered sidewall inlets.

Solver Settings

Assumptions for modeling

Unsteady turbulent flow using a pressure based solver was considered. Standard wall functions were used to model the near-wall viscosity affected regions. The no-slip shear condition was used at the wall domains and the walls were assumed to be smooth.

Simulation Setup

The three-dimensional PDE profile is set up in Fluent. In the Models panel, the VOF multiphase model is turned on. Only pressure-based solvers could be used with the VOF model. The computations use the SIMPLE (Semi Implicit Method for Pressure Linked Equations) or COUPLED algorithm for pressure-velocity coupling and the first-order upwind scheme for the determination of momentum and energy. The settings for the simulations in Fluent can be found in Table 2-3. The time step size Δt was calculated by

$$\Delta t = \frac{\delta x}{V}$$

where δx is the cell size and V is the velocity.

A time step size of 10^{-5} s was used for the beginning of the simulations. Depending on the percentage of fuel in the domain and observing the residuals, this was increased to 10^{-3} s. For spatial discretization, a first-order upwind scheme was used. The summary of the solution methods are displayed in Table 2-4.

Table 2-3 Basic settings of CFD simulation

Parameters/Models	Settings
Spatial and Time settings	3-D Simulation Gravity enabled
Solver	Pressure based solver Absolute velocity formulation Transient state analysis
Turbulence model	Realizable *k*–ε
Multiphase model	Activated with two phases
VOF model	Phase 1: Air Phase 2: Stoichiometric fuel/air mixture Implicit scheme Implicit body forces activated
Time step size	10^{-3} s

Table 2-4 Solution Methods Setting

Solution Methods	Settings
Pressure-Velocity coupling	Simple/Coupled
Gradient	Least squares cell based
Pressure	Presto
Momentum	First order upwind
Volume Fraction	First order upwind
Turbulent kinetic energy	First order upwind
Transient Formulation	First order implicit

Boundary conditions

The uniform inlet velocity was varied from 40 to 180 m/s in increments of 10 m/s. A pressure outlet condition was implemented in order to achieve convergence as it was more stable than outlet vent condition. Additional boundary condition had to be setup for fuel distribution in the domain at the inlet conditions. A summary of the boundary condition is displayed in Table 2- 5.

Table 2- 5 Boundary conditions

Boundary Conditions	**Settings**
Inlet	Mixture: Uniform inlet velocity of 40–180 m/s in increments of 10 m/s Phase 2 (Fuel): volume fraction =1
Symmetry	The lower domain since only half of the PDE is modeled
Wall	No slip
Outlet	Pressure Outlet

Convergence criteria

When the difference between the process values attained at two consecutive iterations was less than the residual amount set, the solution was considered to be converged. The imbalance of the linear discretized equations are known as residuals. The default values of the residuals set by Fluent were sufficient for the given problem statement.

The normalized equation residuals for momentum, continuity, volume fraction and turbulence were monitored to drop below 10^{-3} as shown from Figure 2-16–Figure 2-

20. However, the validity of the solution cannot be judged based on this criterion alone. The difference in the mass flow in and out of the domain should be less than 0.001%. This was verified by setting monitors for mass weighted average as shown in Figure 2-21. The mass flow rate was verified for the initial velocity profiles.

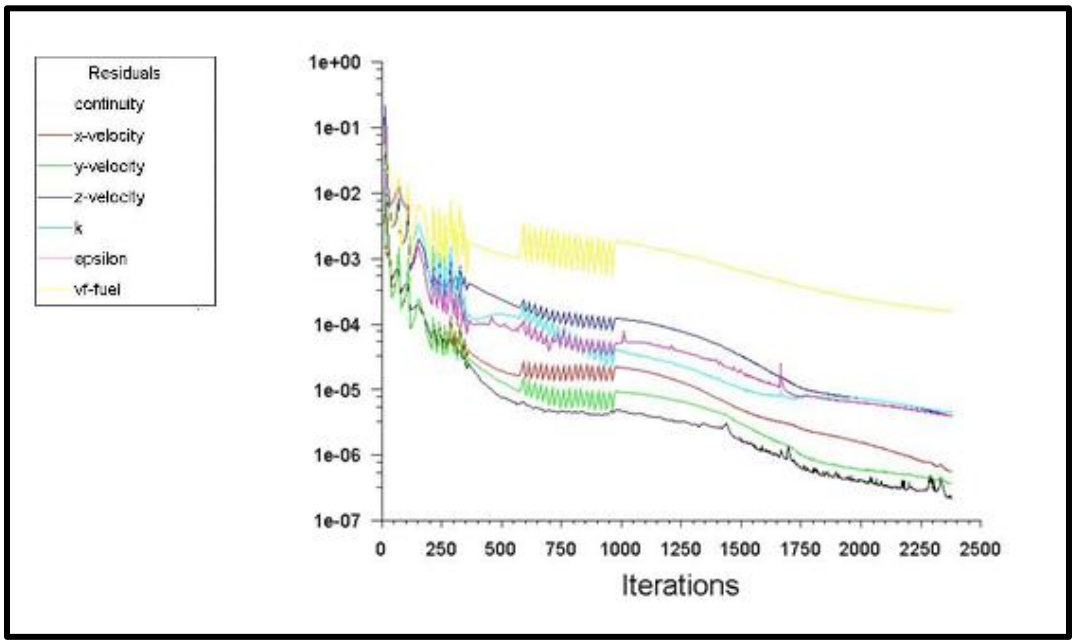

Figure 2-16 Case 1 residual plot

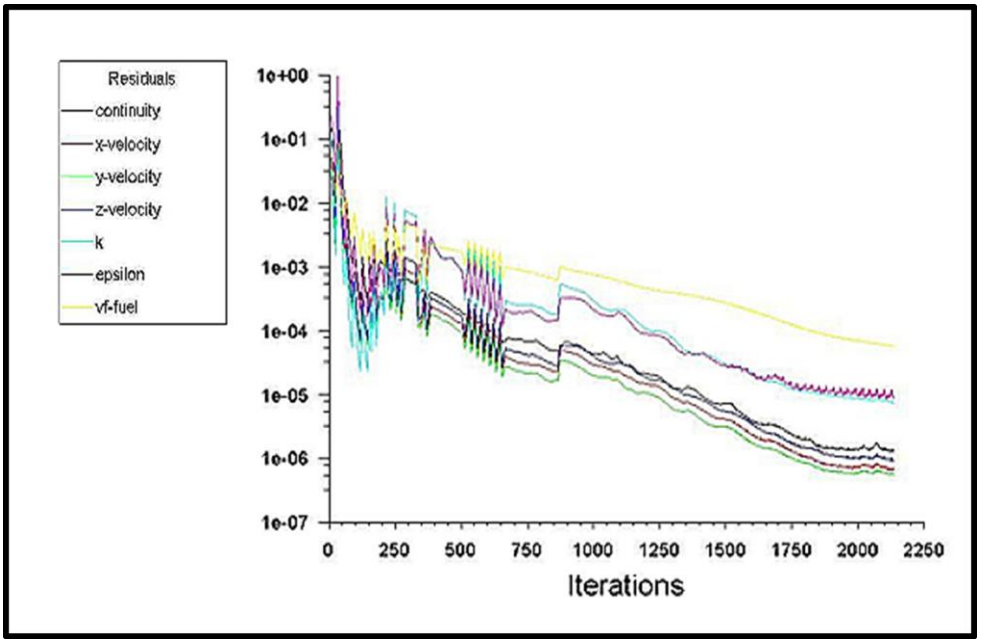

Figure 2-17 Case 2 residual plot

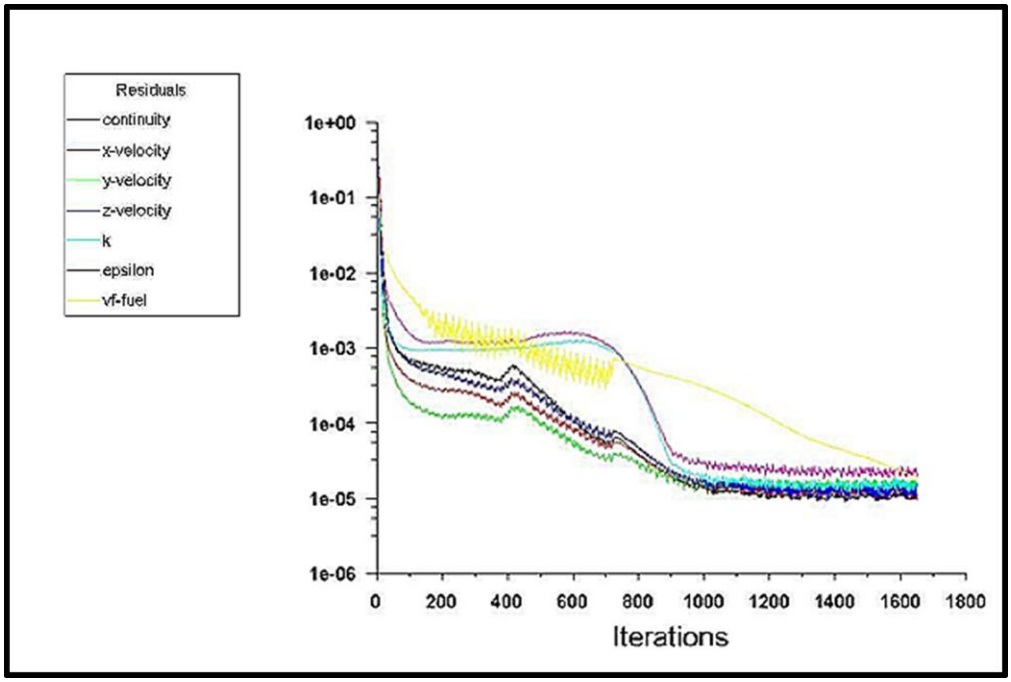

Figure 2-18 Case 3 residual plot

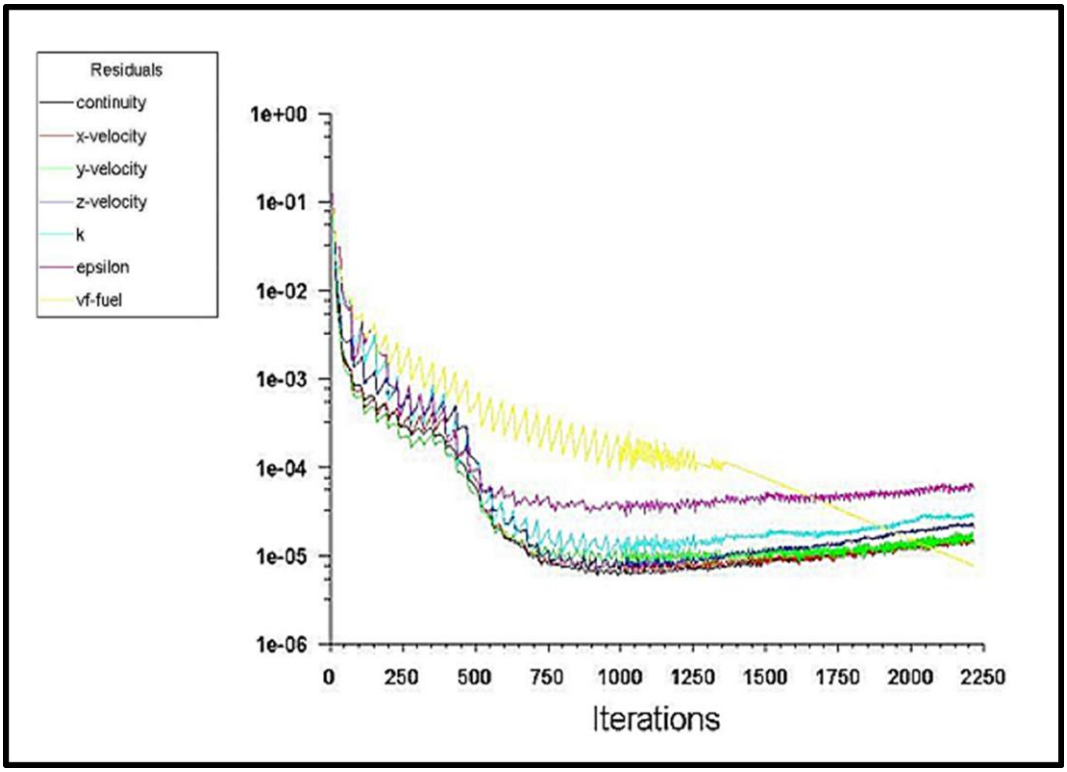

Figure 2-19 Case 4 residual plot

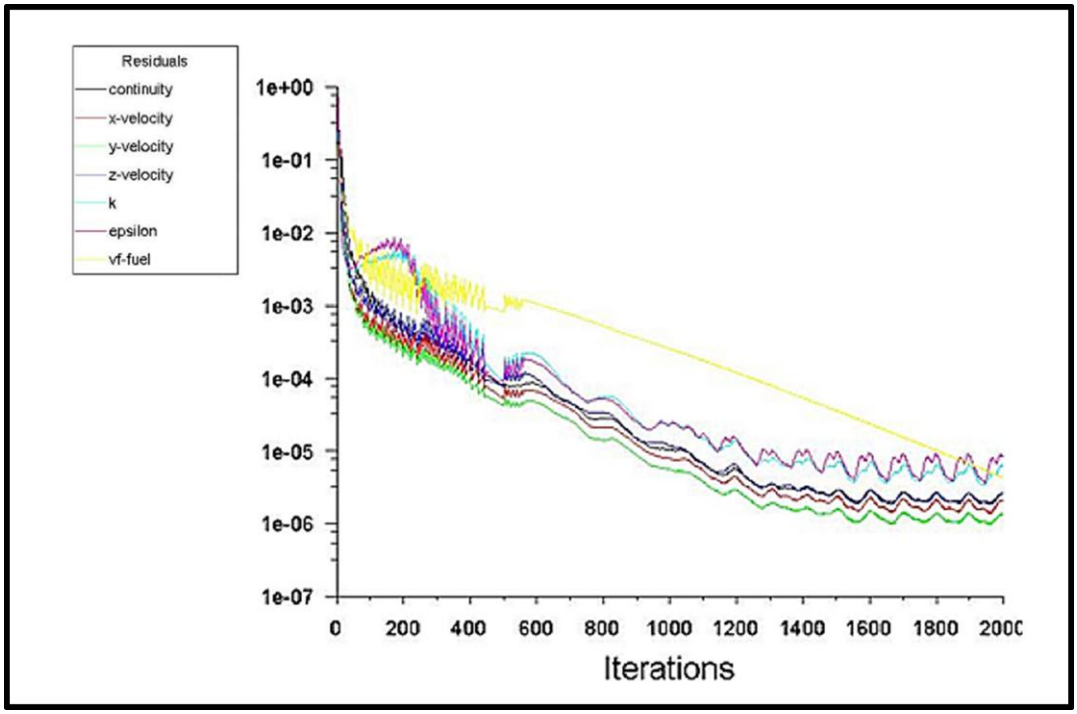

Figure 2-20 Case 5 residual plot

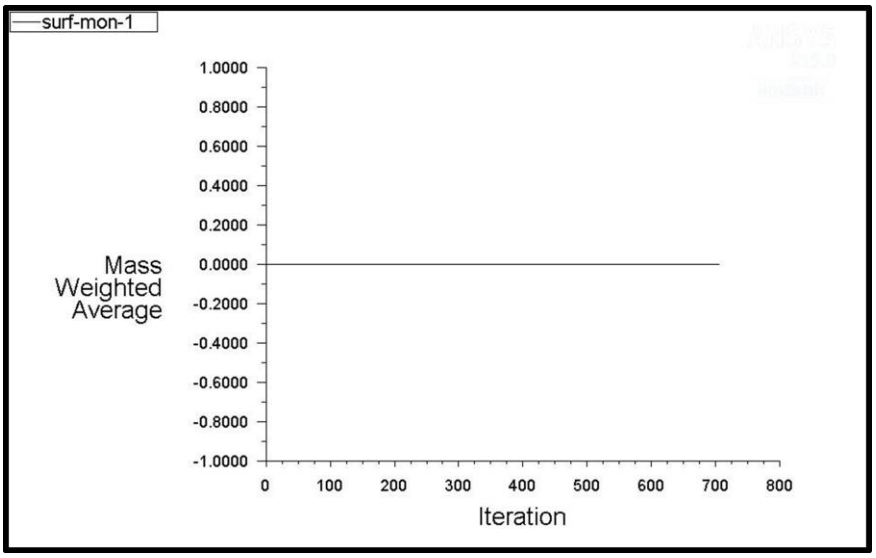

Figure 2-21 Mass Weighted Average

Evaluation Criteria

The simulations were evaluated for their accuracy, time requirement and numerical stability. A grid independence study was carried out for the optimized case 5 for checking the accuracy of the predicted results. The accuracy of the study will be elaborated in the results and discussion chapter. The computation time was 12–14 hours for an individual profile setup using Fluent 15.0^{TM} and Intel Core i7 processor. The simulation was judged to be good due to small run times for all cases except case 2 which made use of a slightly coarser mesh. The numerical stability is generally evaluated on the difficulty to obtain a converged solution. There was no need to reduce the under-relaxation factors or other methods for stabilizing the solution in order to achieve convergence. Thus, the simulation was presumed as good with respect to stability.

Chapter 3

Results and Discussion

Case 1

In order to visualize fill process, a symmetry plot of the fuel volume fraction was obtained using CFD-Post™ for progressive time steps as displayed from Figure 3-1– Figure 3-3 for different reactant mixtures introduced at 40 m/s from the port on the left. The criterion for the fill time was considered at 90% fill fraction volume. The data are available in Appendix A. Hydrogen-air requires the maximum fill time of 2.11 s for case 1 whereas methane-air takes the least at 1.90 s. Propane-air and octane-air had similar fill times of 1.93 s.

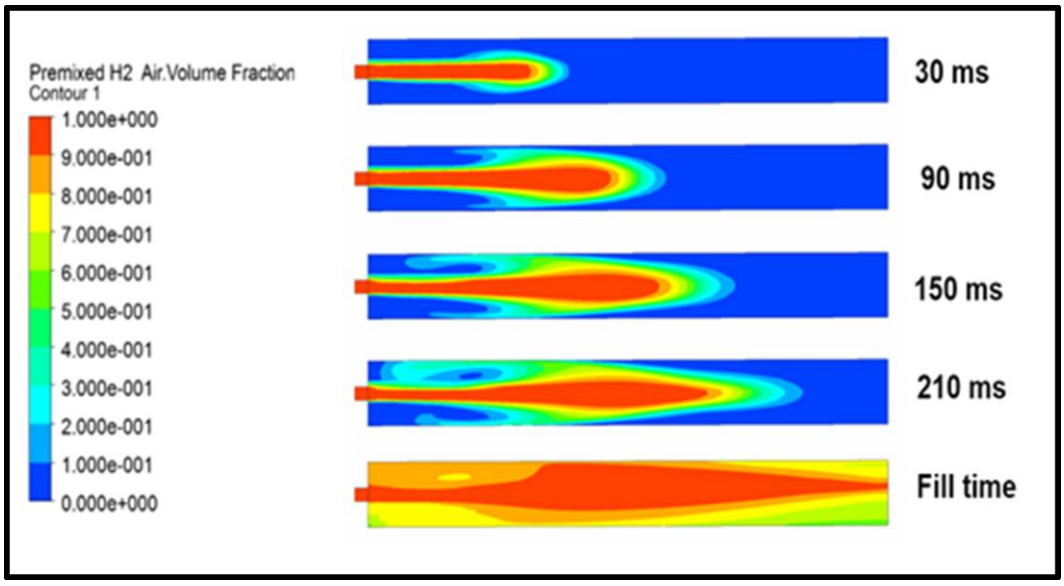

Figure 3-1 Case 1- hydrogen-air volume fraction contours

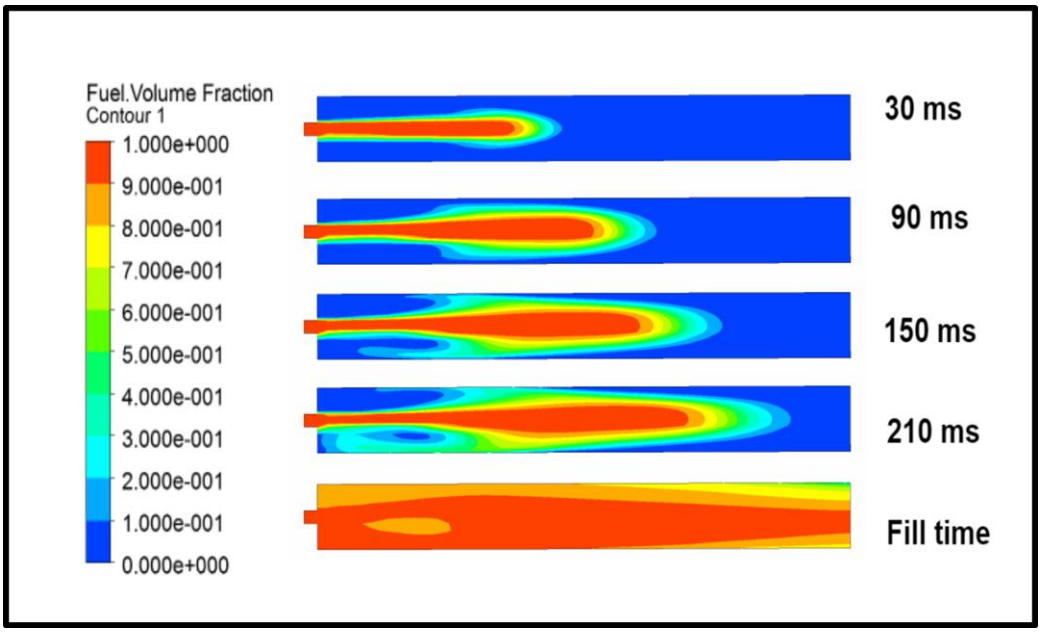

Figure 3-2 Case 1- propane-air volume fraction contours

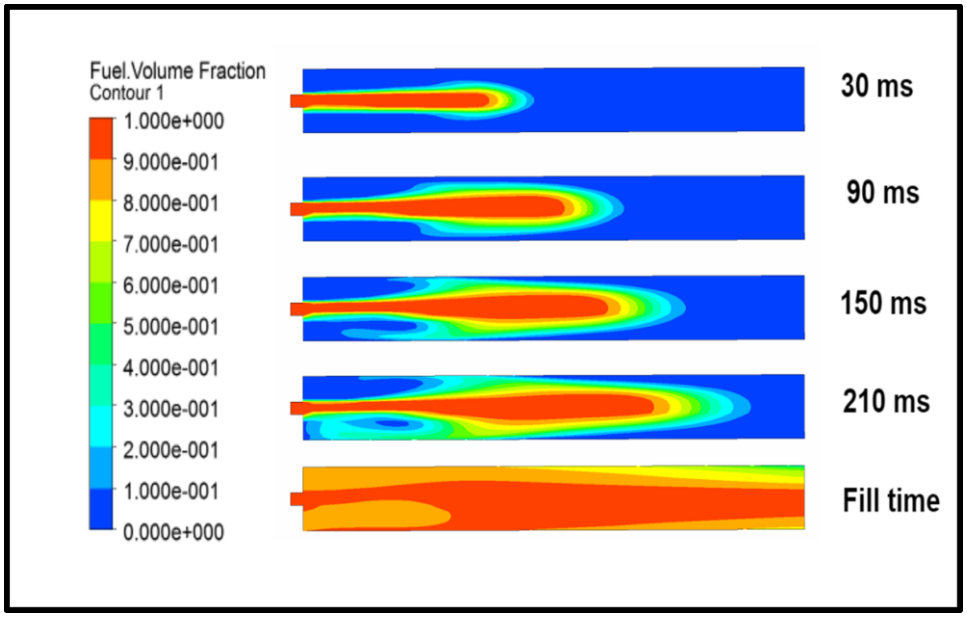

Figure 3-3 Case 1- octane-air volume fraction contours

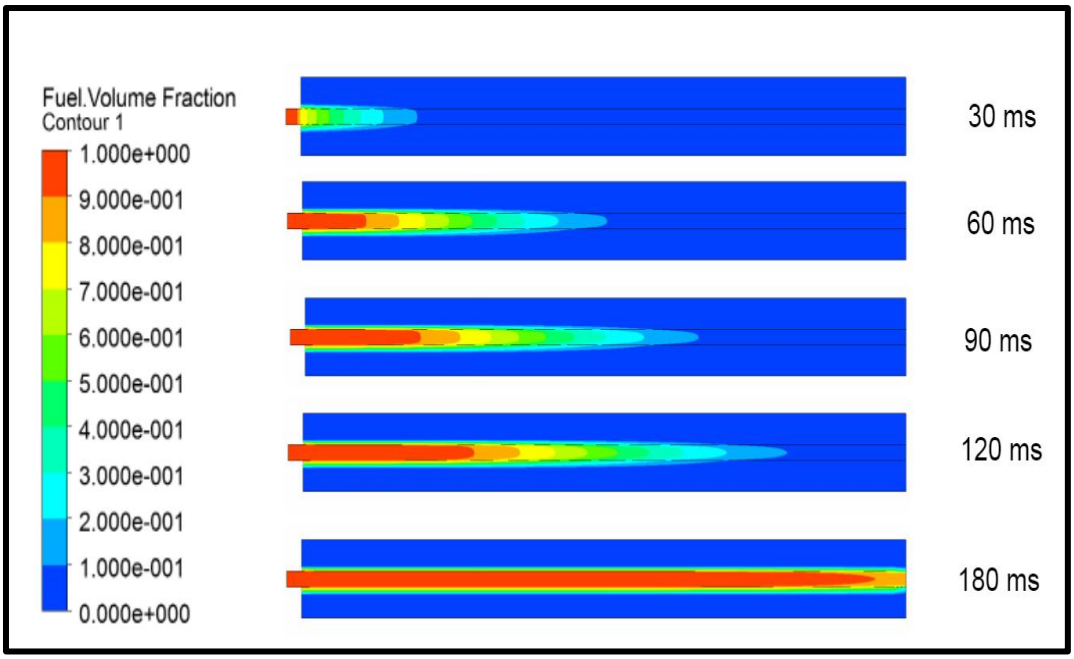

Figure 3-4 Case 1- hydrogen-air filling profile at 180 m/s

The fuel injected from the main inlet has a profile like that of a confined jet. This is illustrated better at higher velocities (180 m/s) as can be seen in Figure 3-4. The Case 1 geometry did not seem efficient enough to eliminate the isolated pockets of air. This difficulty will be elaborated in the subsequent sections.

Case 2

The reactant mixture from the side inlets impinged against the flow from the main inlet. It was this breaking up of the flow for the four side inlet configurations which yielded different simulation results. This geometry resulted in the most reduced filling time using a fill criterion of 90 percent volume fraction. However, the presence of dead air regions close to the closed end of the PDE could still not be avoided. Figure 3-5 and Figure 3-6

display the filling profiles for the various reactant mixtures. Hydrogen-air had the least fill time of 230 ms whereas all the other fuels had similar filling times of 250 ms.

Case 3

Generally, this configuration takes more time to fill than for case 2. However, the presence of the dead air regions was eliminated to a larger extent as can be seen in comparing Figure 3-6 against Figure3-7 .The fill time was highest for propane-air at 448 ms and lowest for octane-air with 428 ms.

Case 4

The air gaps were reduced significantly in comparison with case 2. However the filling time was larger than case 3 configuration. Octane-air had the highest fill time of 640 ms and hydrogen-air had the least fill time at 250 ms.

Case 5

This configuration was considered a perfect balance for a reasonable amount of fill time and had the least amount of dead air regions. The filling volume study in the upcoming section emphasizes this.

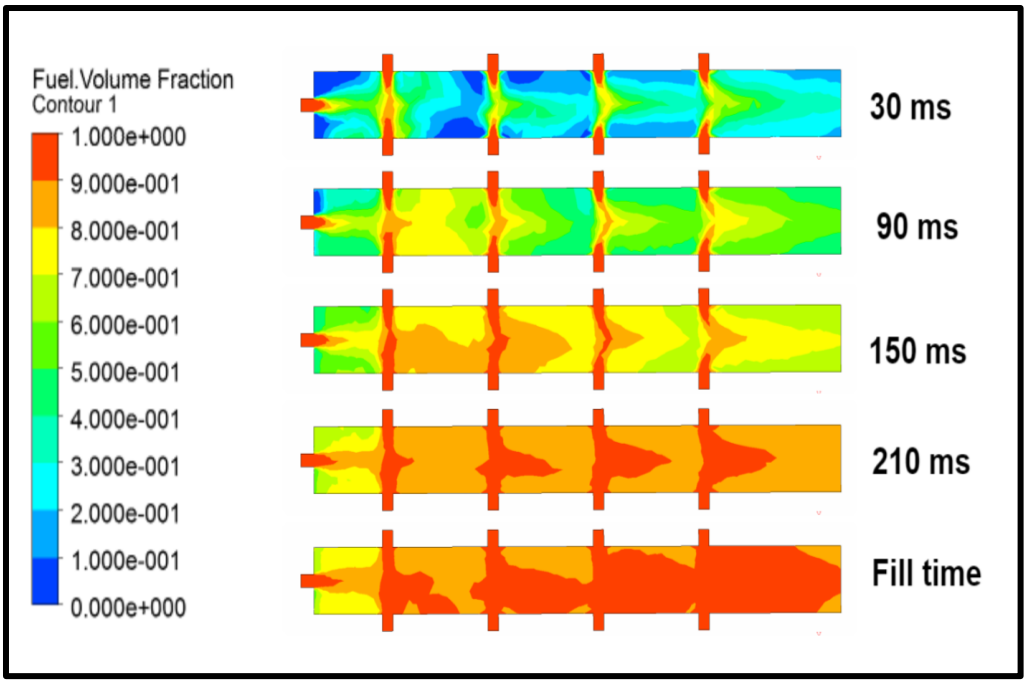

Figure 3-5 Case 2- methane-air volume fraction contours

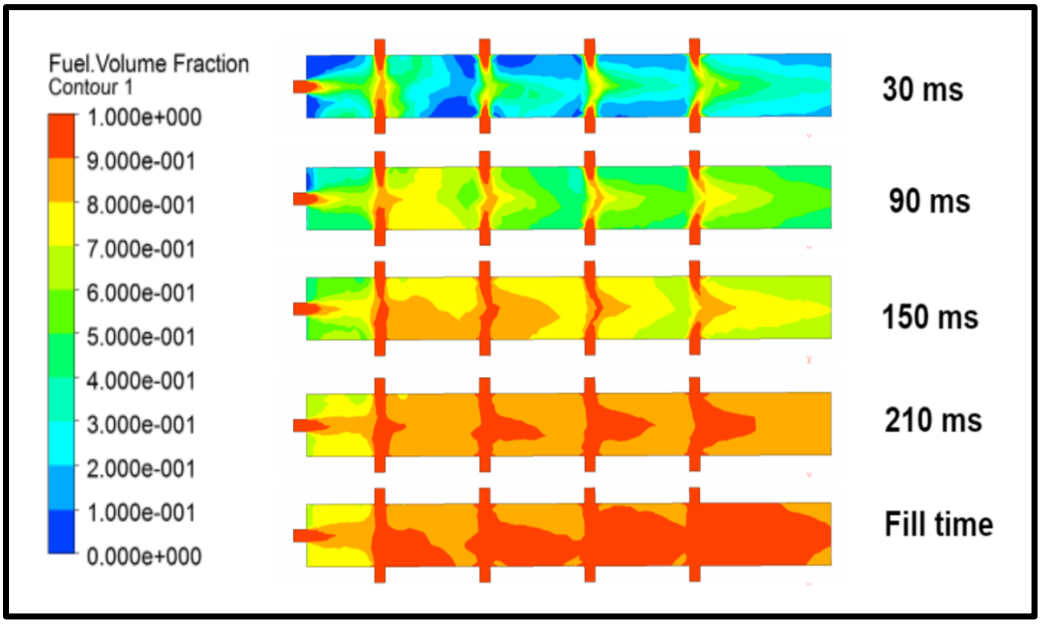

Figure 3-6 Case 2- octane -air volume fraction contours

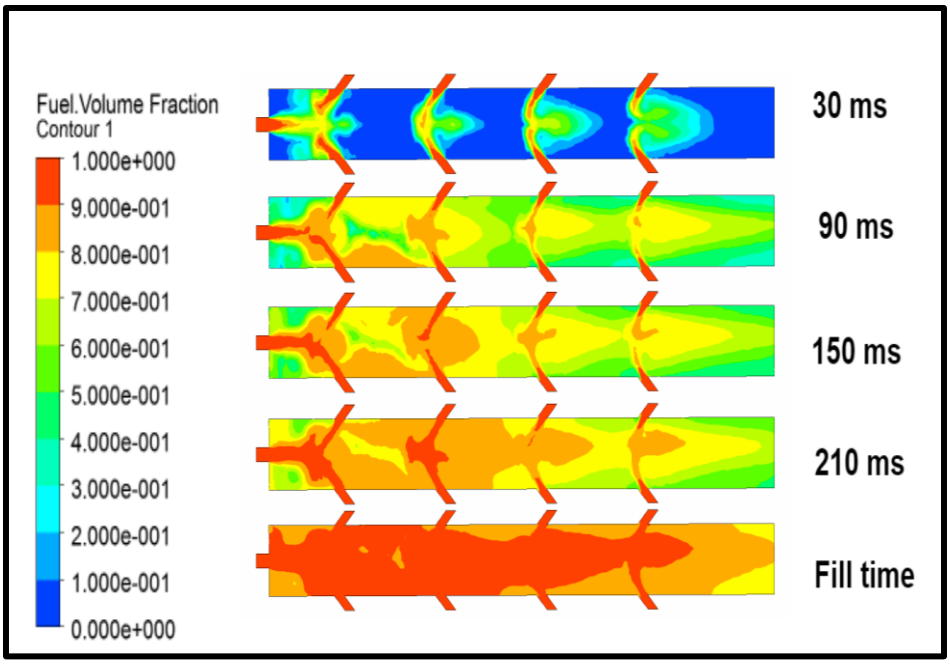

Figure 3-7 Case 3- octane-air volume fraction contours

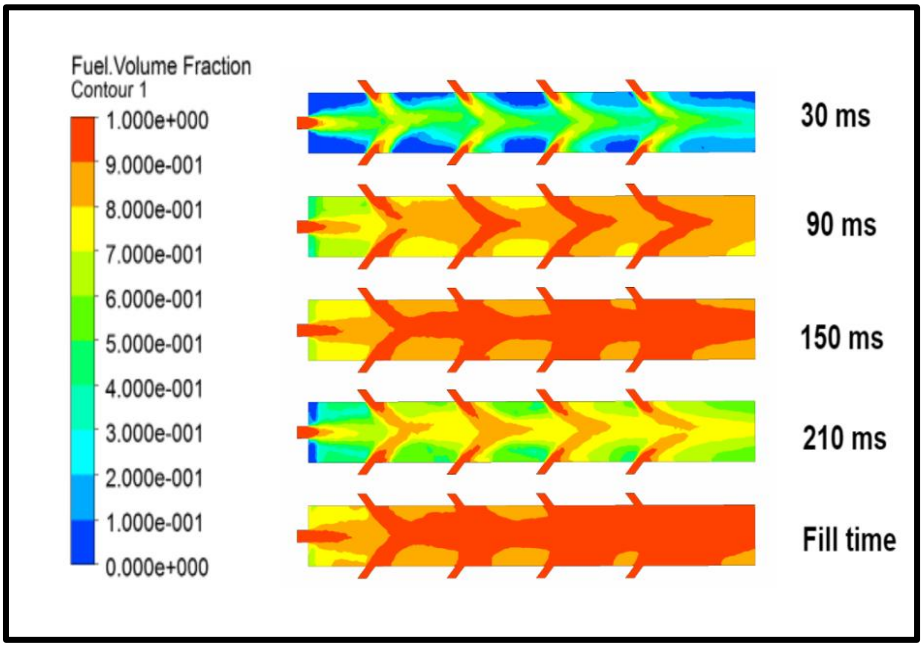

Figure 3-8 Case 4- biogas-air volume fraction contours

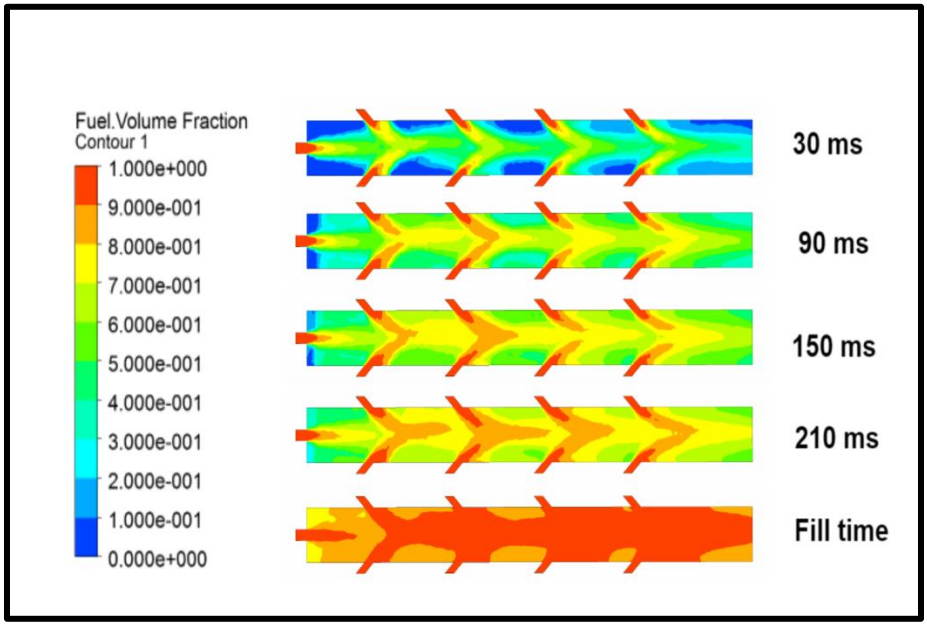

Figure 3-9 Case 4- methane-air volume fraction contours

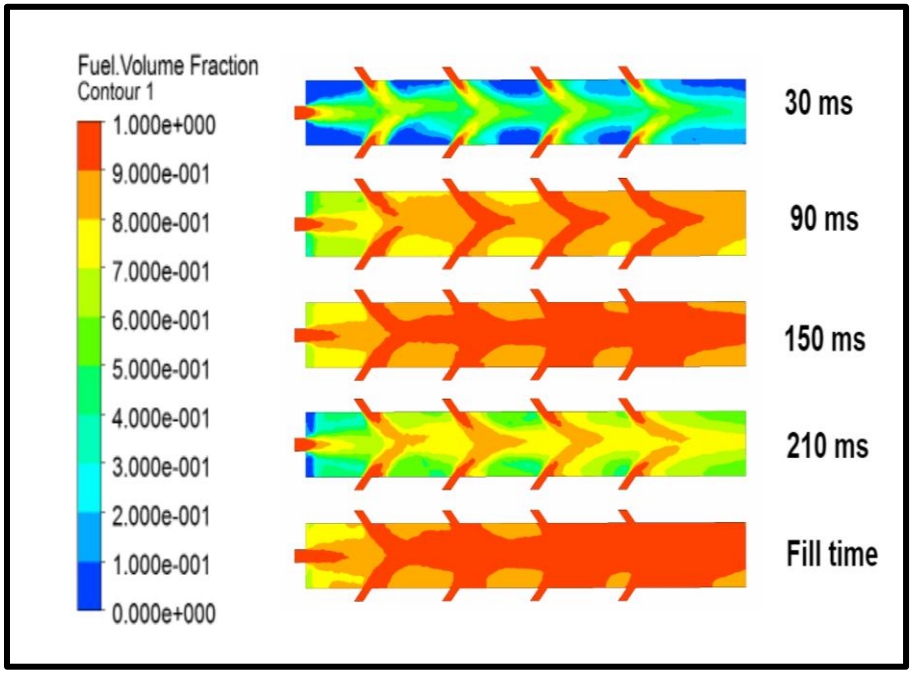

Figure 3-10 Case 4- octane-air volume fraction contours

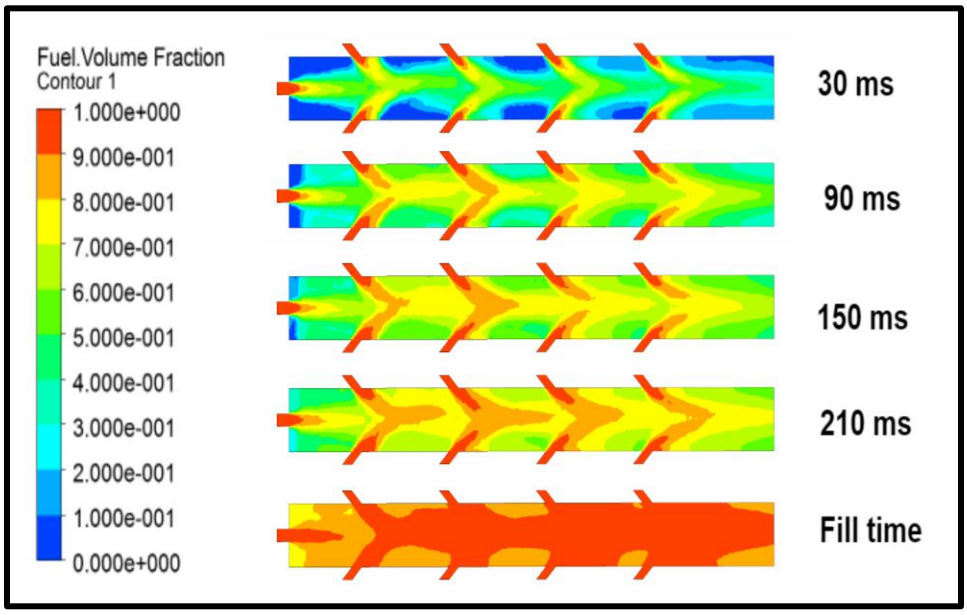

Figure 3-11 Case 4 - propane-air volume fraction contours

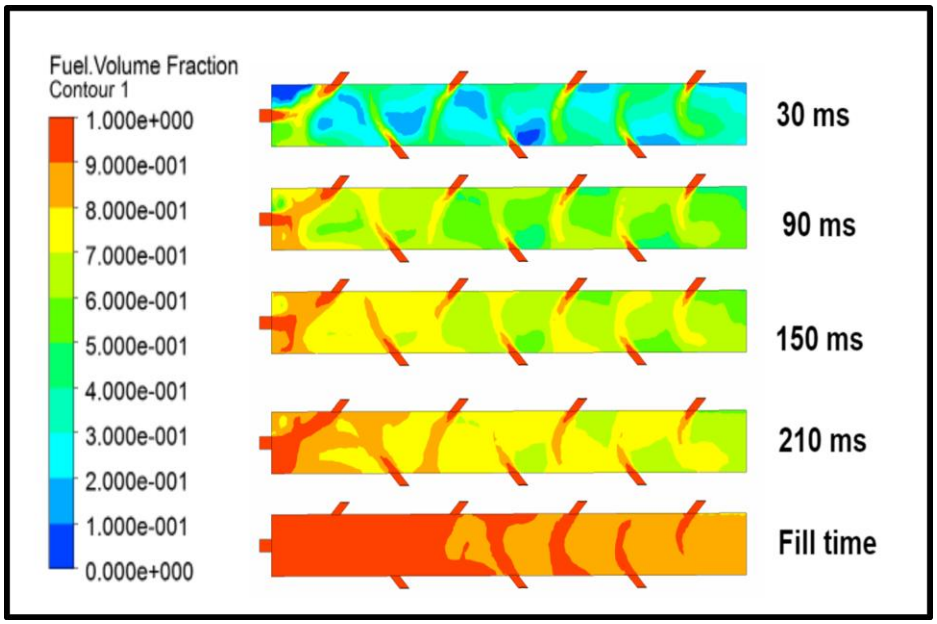

Figure 3-12 Case 5- octane -air volume fraction contours

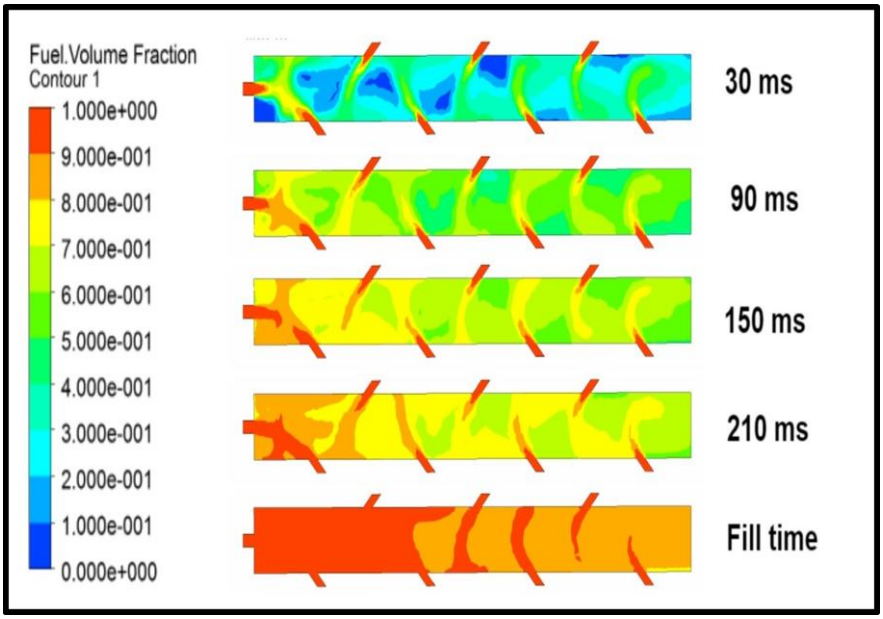

Figure 3-13 Case 5- biogas -air volume fraction contours

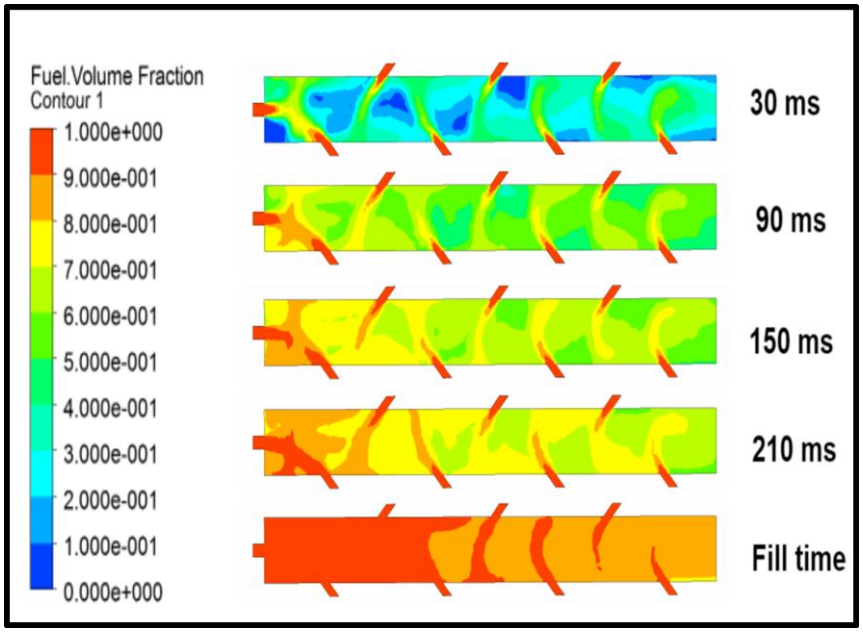

Figure 3-14 Case 5- propane -air volume fraction contours

Filling time study

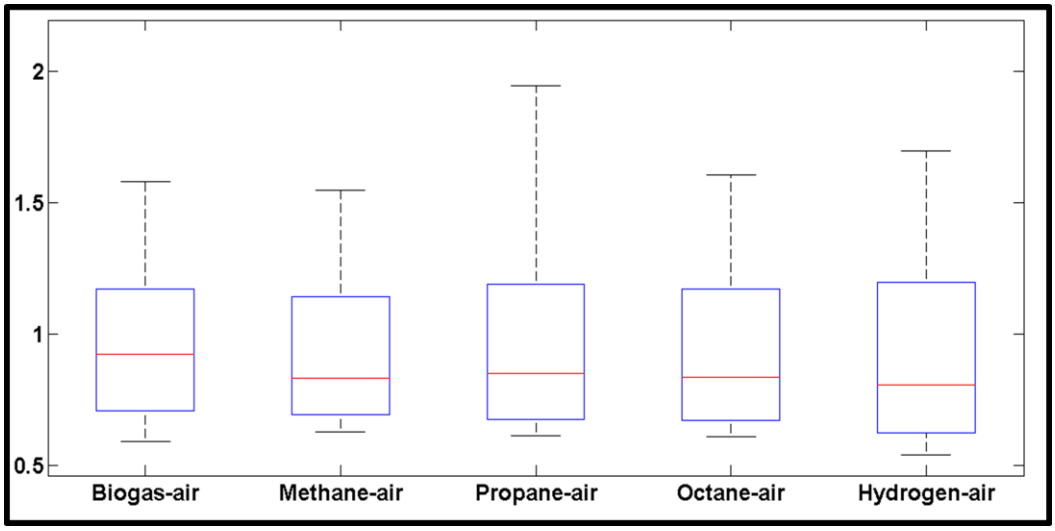

Figure 3-15 Case 1- filling time distribution

The filling times for velocities ranging from 40–180 m/s in increments of 10 m/s areshown in Figure 3-15–3-20 in the form of box plots. Refer to Appendix A for the data listing. The distribution gives an insight on the different filling times for the 5 different fuel-air mixtures used. Figure 3-15 corresponds to case 1, with just one inlet. The top and the bottom of the box represent the 75^{th} and the 25^{th} percentiles of the mixture fill time respectively. The middle line in the box shows the median of the distribution. The lower quartile represents the filling times for higher velocities and the upper quartile represents the filling times for lower velocities. The upper and lower whiskers mark the velocities 40 and 180 m/s respectively. At higher velocities, hydrogen-air filled faster whereas at lower velocities, methane-air filled much faster than the other mixtures.

The box plot for case 2 is shown in Figure 3-16. The distribution is similar to that of case 1. At lower velocities, Biogas/air took the maximum fill time whereas hydrogen/air takes the minimum fill time at both higher and lower velocities.

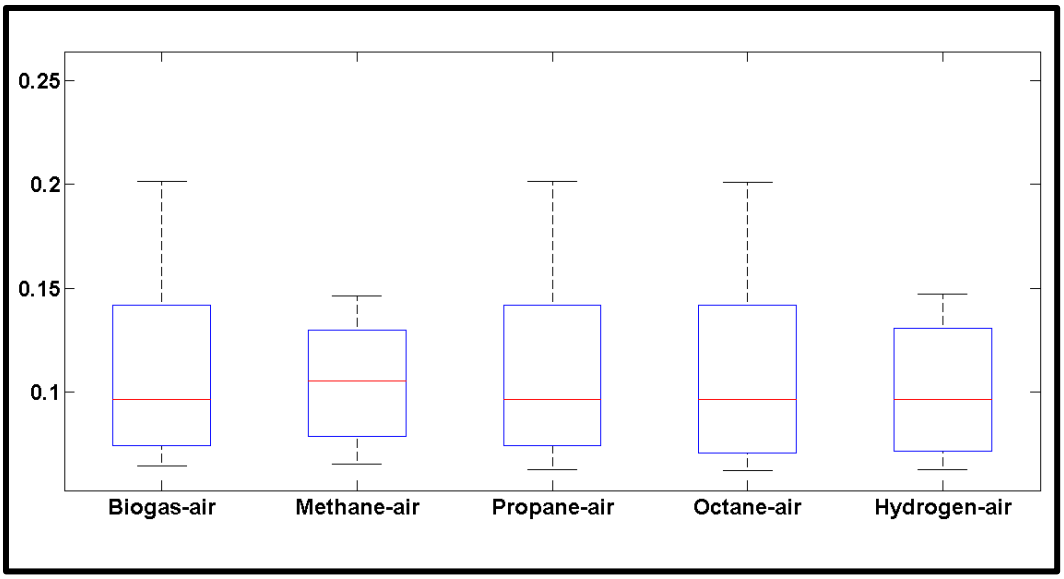

Figure 3-16 Case 2- filling time distribution

The fill time distribution for case 3 is shown in Figure 3-17. Propane-air showed severe variations and hydrogen-air had the least fill time at both higher and lower velocities.

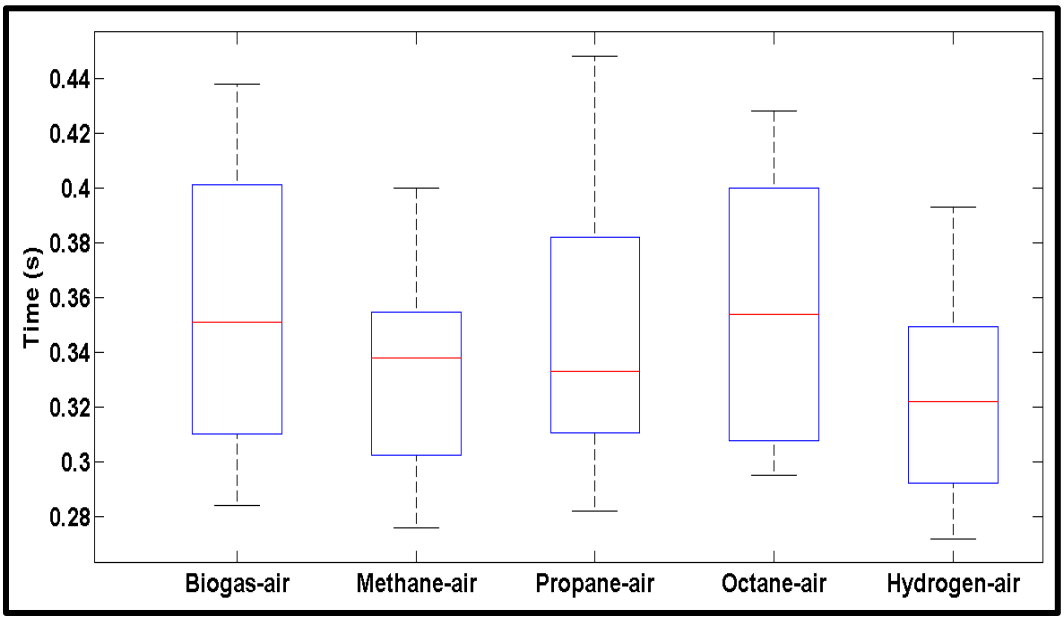

Figure 3-17 Case 3- filling time distribution

The box plot for case 4 in Figure 3-18 shows severe variations in the fill time. Hydrogen-air has the least fill time at both lower and higher velocities. Methane-air, propane-air

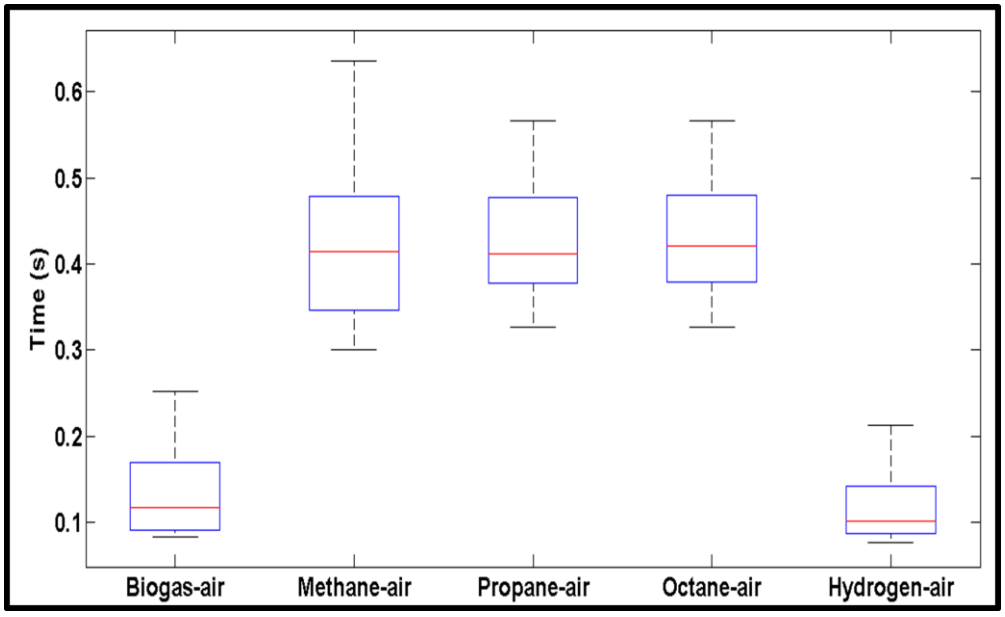

Figure 3-18 Case 4- filling time distribution

and octane-air have similar filling time at higher velocities. For case 5, octane-air had the least fill time at all velocities. Hydrogen-air could be considered as the optimum mixture from all the case studies.

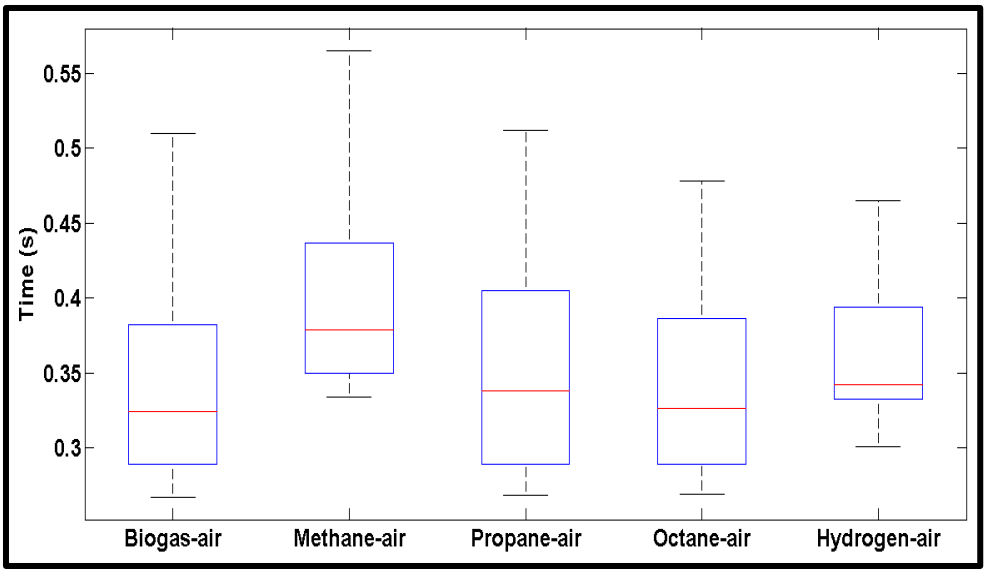

Figure3-19 Case 5-Filling time distribution

Filling Volume Study

Figure 3-20–Figure 3-23 below show the filling volume and the corresponding volume of dead air region at a given time. From the figures, it can be understood that when there is no mixture, the chamber is filled with air and when the mixture is being filled, the dead air region reduces. Cases 1, 3, 4 and 5 discussed in the problem statement were compared. The idea of this comparison is to show which case eliminates the dead air regions the most and at what optimum filling time is it being accomplished. All the cases were compared for the same velocity of 120 m/s and with an octane-air mixture in order to maintain consistency. The point where the fuel volume reaches 0.9 was taken as the filling criterion and the time and volume of dead air region at that point were compared.

Case 1

With just one inlet, case 1 has a filling time of about 0.9 s and it still has a considerable amount of dead air region left as shown in Figure 3-20.

Cases 2, 3 and 4

Case 2 had the lowest fill time; however, the presence of air gaps near the PDE entrance was already illustrated in the volume fraction contours. Cases 3 and 4 reached the fill criterion in a very short time but the dear air region volume was significantly higher.

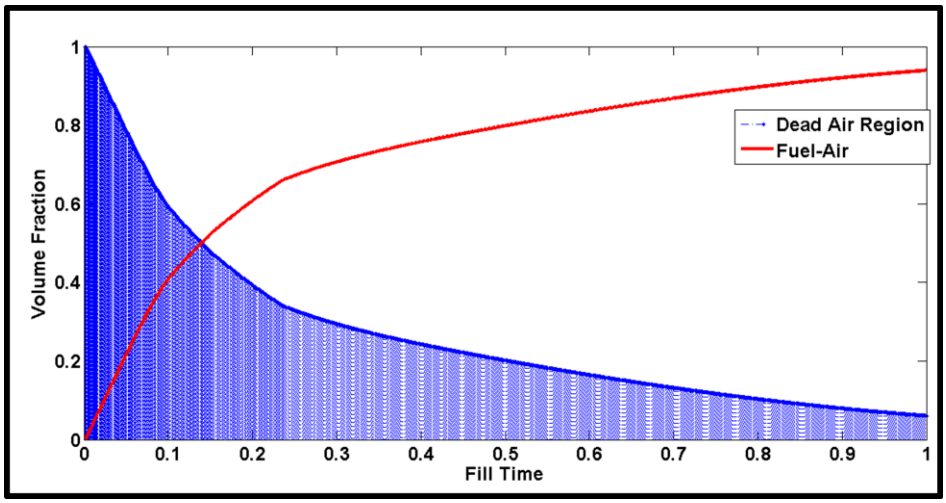

Figure 3-20 Case 1- Volume filling

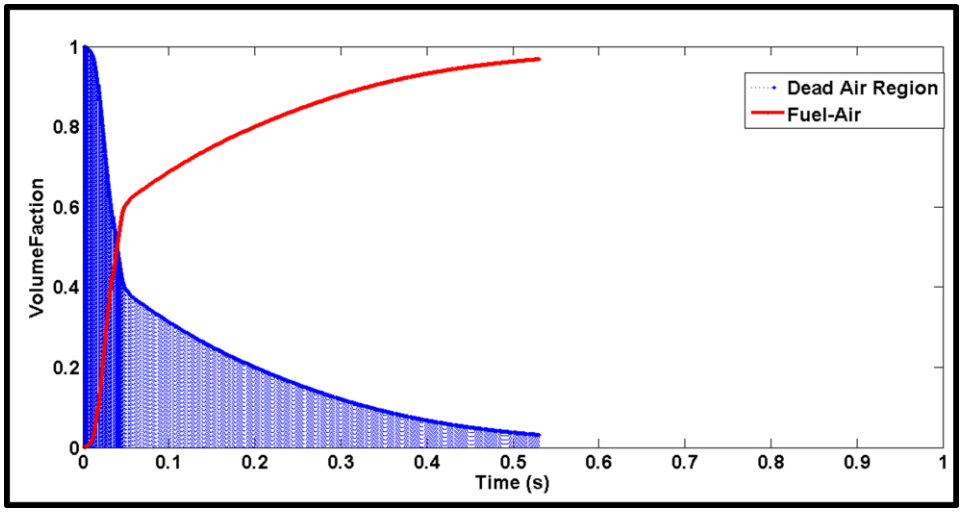

Figure 3-21 Case 3- Volume filling

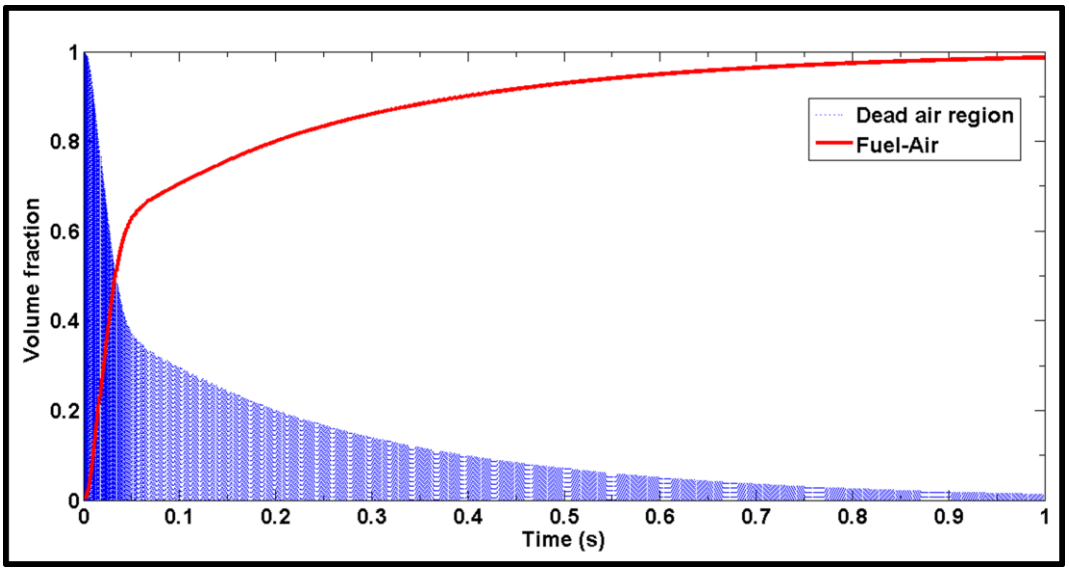

Figure 3-22 Case 4- volume filling

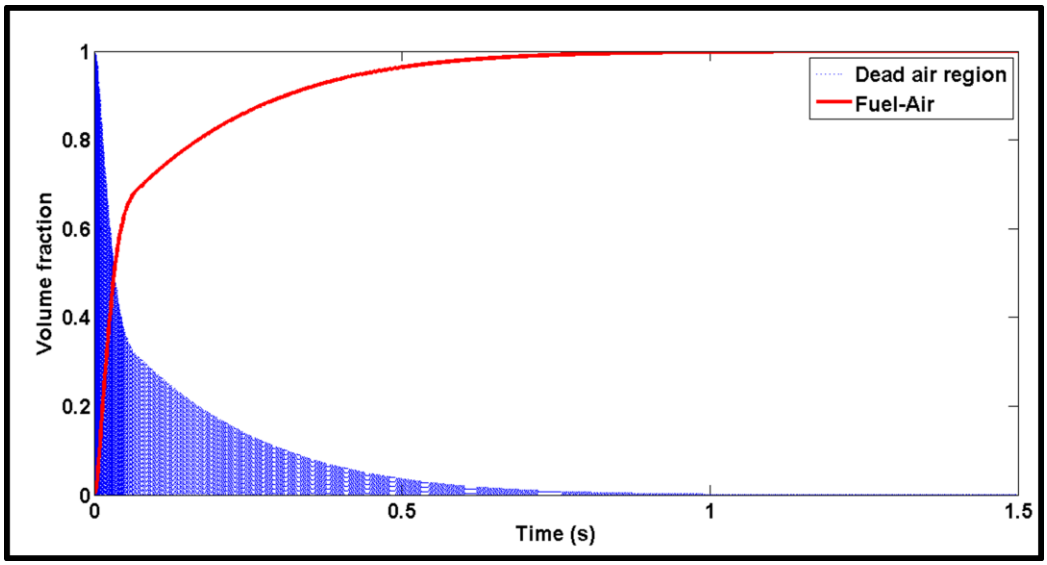

Figure 3-23 Case 5- volume filling

Case 5

The reduction in air gaps was faster for case 5 as shown in Figure 3-23. It also yielded the least fill time. Case 5 proved to be the most optimum design as it eliminates most of the dead air region at a relatively shorter time as seen in Figure 3-24.

Case Optimization

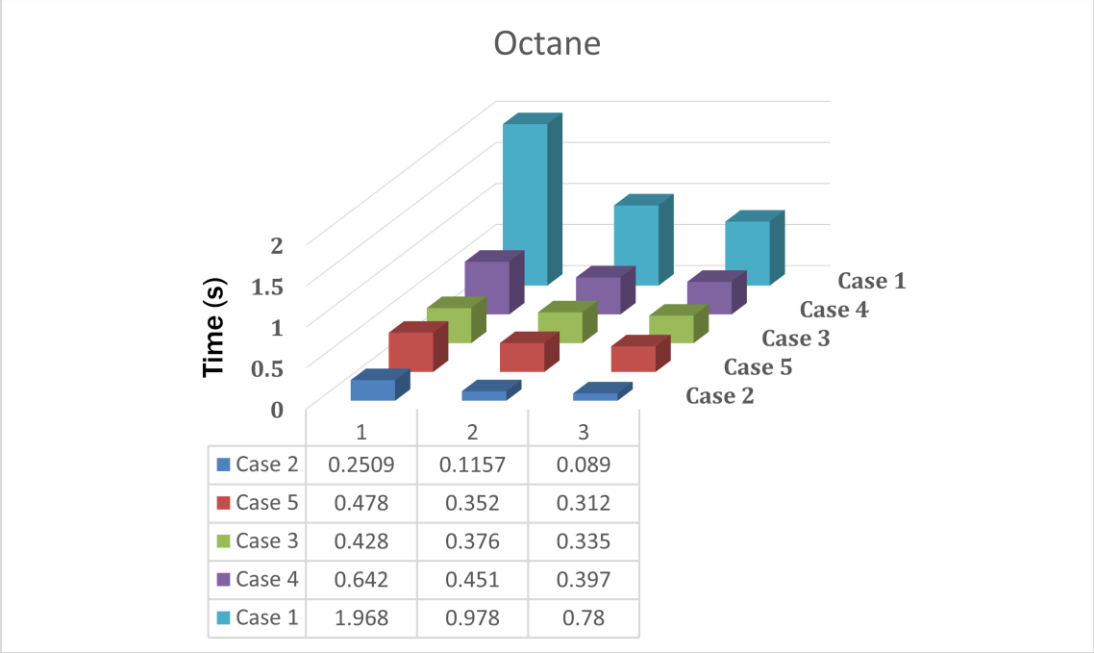

Figure 3-24 Case optimization

For the octane-air mixture, the data for all the five cases were compared for the velocities 40, 90 and 120 m/s as can be seen in Figure 3-24. Case 2 had the least filling time for all the 3 velocities and case 1 had the maximum filling time. Cases 3 and 5 were in close comparison, but case 5 had the least filling time in each velocity profile. Hence,

it can be confirmed that case 5 was the most optimum in terms of filling time for any given velocity and fuel.

Sensitivity Analysis

In order to make sure that the selected settings are suitable for the studied flow, a sensitivity analysis was performed. The properties inspected during the sensitivity analysis were:

Mesh Independence

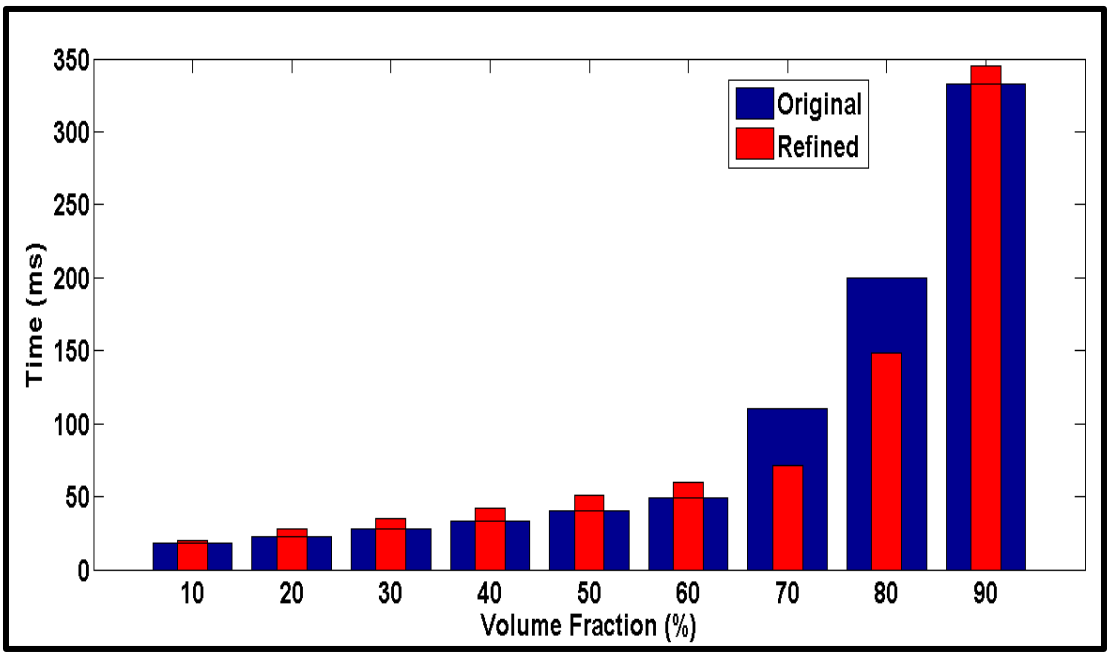

Figure 3-25 Percentage fill fraction difference

Table 3-1 Original and refined mesh

Case Points	Tetrahedral cells	Pyramid cells	Prism cells	Total cells	Total points
Original	380,897	0	15,240	396,137	86,748
Refined	571,262	0	15,240	586,502	122,208

Inorder to perform a mesh independence study, the size of the mesh was increased to 600,000 cells. This was done by changing the grid spacing near the wall domains for better interface capture.

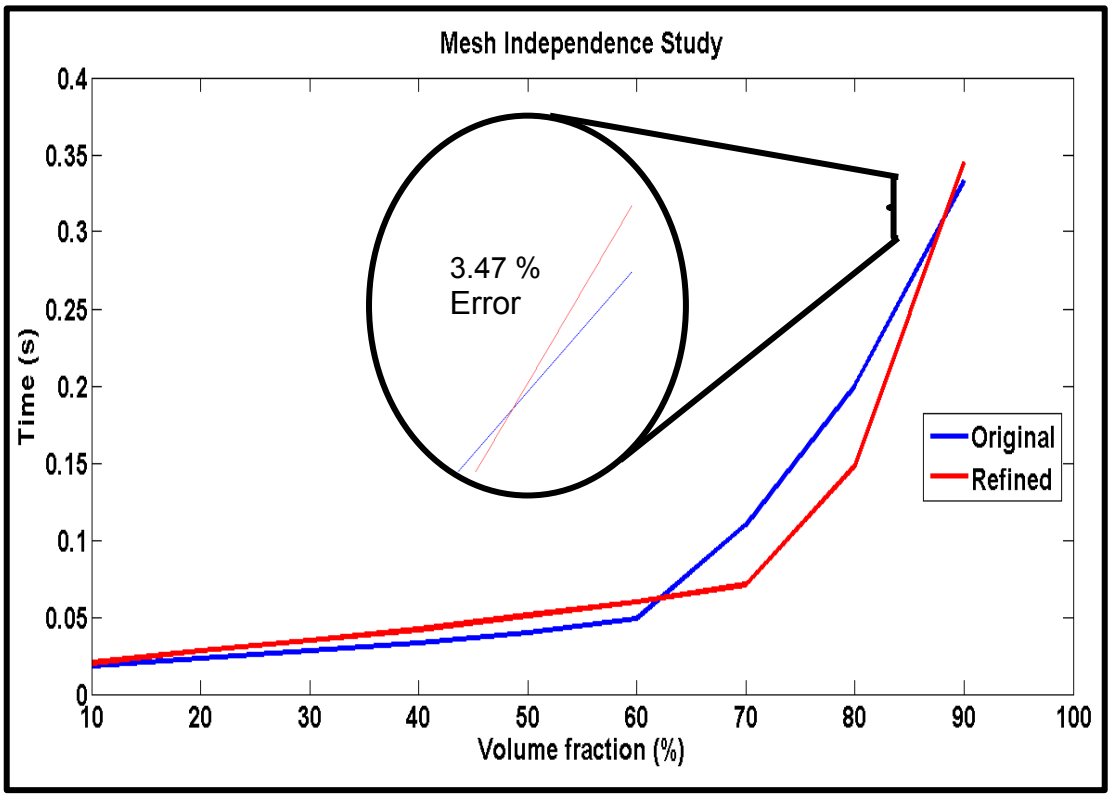

Figure 3- 26 Percentage error at fill criterion

Table 3-1 shows the two mesh types used in the study.The fuel filling percentages were plotted in Figure 3-25 for the two cases for a velocity of 120 m/s with octane. The two filling profiles for both the original and the refined mesh closely follow each other. The least amount of difference was found at the 10 percentage fill fraction. At the filling criterion i.e., at 90% fill fraction, the difference was 3.47%. Thus, it could be concluded that overall the results were independent of the mesh resolution.

Discretization scheme

The coupled solver was analyzed for the same setup in addition to the segregated solver for case 5 which was more stable. Figure 3-27 was obtained using the actual time taken for filling and the fill time difference between the coupled and segregated solver. For all the three fuel-air mixtures compared, the trend lines are similar at higher velocities, although the methane-air has a relatively higher margin of error at 120 m/s. Biogas has the least margin of error at all the three velocities while the methane-air mixture has the highest margin of error of 6%.

Turbulence Model Spatial Discretization

All the preceding presented results were computed with a first-order upwind scheme for the turbulence kinetic energy (k) and dissipation (ε). The first-order upwind scheme was more robust than the second-order. However, diffusion was overestimated with first-order upwind schemes. This analysis was performed to evaluate how the numerical scheme for turbulent kinetic energy and dissipation affects the results. The flow was not affected by the change of numerical scheme. Figure 3-28 shows the error comparison of first- and second-order turbulence spatial discretization schemes for Biogas, methane and octane. Methane-air had the largest error of 4% at 90 m/s.

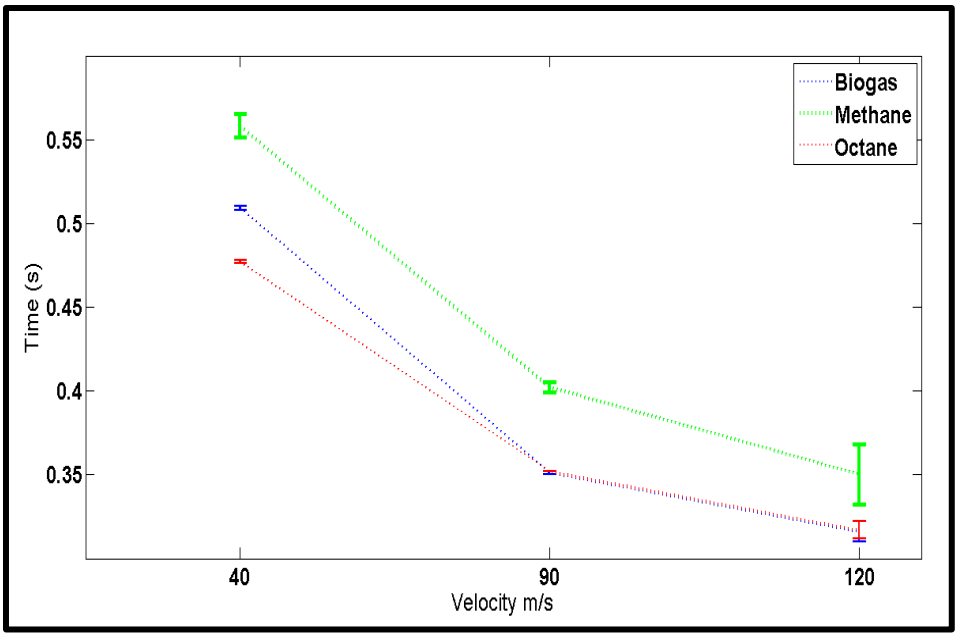

Figure 3-27 Coupled vs Segregated Work

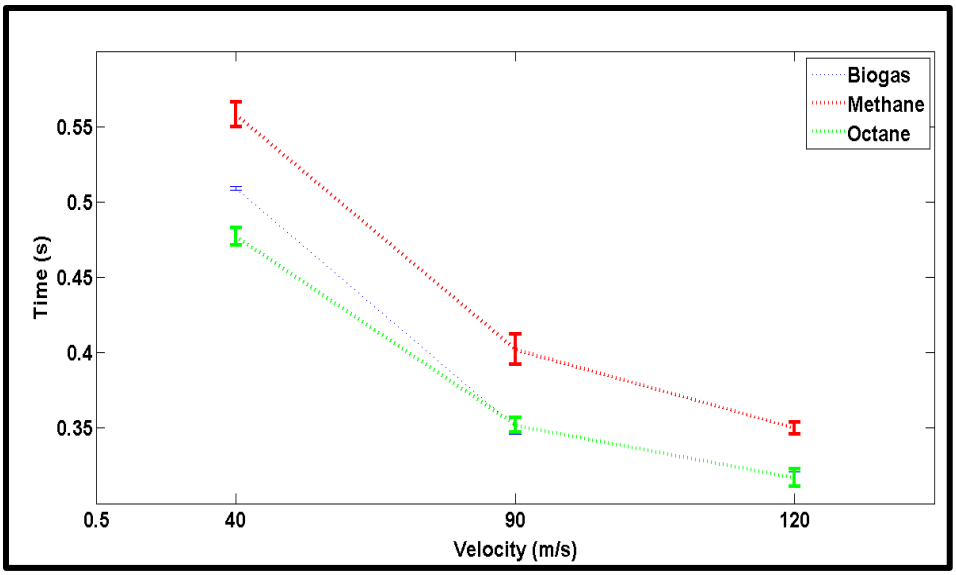

Figure 3-28 Turbulence Numerical Scheme

Conclusions and Future Work

The recommendations from this research were based on the comparison of the 5 different cases. Case 5 was the most promising case from this comparison. Hydrogen-air had the least fill time from the fuel optimization results.

The results presented emphasize the possibilities in simulation of filling process of PDE with the Volume of Fluid model. The implicit VOF discretization scheme was more stable and less computationally expensive than the explicit VOF model. The present work is purely numerical and experimental validation will be valuable. The experimental approach will require a detailed monitoring of the reactants which will be extremely demanding.

A more sophisticated large-eddy simulation may be useful to determine the degree of mixedness especially the interface between the reactants and the initial volume of air. A more sophisticated injector head geometry for staggered side-ports might yield better results. The possibilities for phase injection could also be explored.

Appendix A

Result Table

The results for all the case runs at different velocities and fuels are tabulated. These times in seconds are when the PDE was filled with 90% of the fuel-air premixed composition.

Case 1

Velocity	Biogas-air	Methane- air	Propane- air	Octane- air	Hydrogen-air
40	1.936	1.902	1.946	1.968	2.118
50	1.583	1.549	1.608	1.608	1.698
60	1.300	1.329	1.384	1.371	1.429
70	1.203	1.174	1.223	1.204	1.233
80	1.085	1.058	1.098	1.078	1.091
90	1.000	0.968	0.999	0.978	0.978
100	0.923	0.893	0.918	0.899	0.885
110	0.862	0.834	0.85	0.835	0.807
120	0.812	0.787	0.794	0.78	0.744
130	0.995	0.748	Outlier	0.734	0.690
140	0.732	0.716	0.703	0.696	0.641
150	0.700	0.688	0.669	0.663	0.603
160	0.671	0.664	0.641	0.635	0.566
170	0.604	0.644	0.616	0.611	0.541
180	0.590	0.627	0.613	0.61	0.621

Case 2

Velocity	Biogas-air	Methane- air	Propane- air	Octane- air	Hydrogen-air
40	0.2511	0.2515	0.2512	0.2509	0.229
50	0.2014	Divergence detected	0.2014	0.2012	Divergence detected
60	0.1718	Divergence detected	0.15	0.1689	Divergence detected
70	0.1461	0.1461	0.1461	0.1461	0.145
80	0.129	0.129	0.129	0.129	0.125
90	0.1157	0.1157	0.1157	0.1157	0.112
100	0.105	0.105	0.105	0.105	0.101
110	0.0963	0.0963	0.0963	0.0963	0.093
120	0.0892	0.0889	0.089	0.089	0.0845
130	0.0828	0.0827	0.0828	0.0828	0.0799
140	0.0775	0.077	0.0775	0.07	0.0749
150	0.0729	0.0725	0.0729	0.0725	0.069
160	0.0689	0.07	0.0688	0.0685	0.0628
170	0.0654	0.0651	0.0649	0.065	0.0619
180	0.2512	0.1157	0.0623	0.062	0.0588

Case 3

Velocity	Biogas-air	Methane- air	Propane-air	Octane- air	Hydrogen-air
40	0.438	0.4	0.448	0.428	0.42
50	0.433	Divergence detected	0.412	0.414	0.499
60	0.419	0.338	0.379	0.403	0.33
70	0.408	0.353	0.398	0.404	0.32
80	0.380	0.342	0.383	0.390	0.34
90	0.375	0.364	0.365	0.376	0.33
100	0.361	0.355	0.352	0.357	0.33
110	0.351	0.347	0.333	0.354	0.32
120	0.333	0.334	0.32	0.335	0.32
130	0.327	0.324	0.328	0.329	0.31
140	0.320	0.316	0.318	0.307	0.3
150	0.306	0.291	0.306	0.307	0.29
160	0.307	0.298	0.308	0.310	0.267
170	0.289	0.288	0.283	0.295	0.28
180	0.284	0.276	0.282	0.295	0.272

Case 4

Velocity	Biogas-air	Methane- air	Propane- air	Octane- air	Hydrogen-air
40	0.252	0.635	0.64	0.642	0.25
50	0.205	0.549	0.566	0.566	0.23
60	0.175	0.522	0.515	0.527	Divergence detected
70	0.154	0.489	0.486	0.487	Divergence detected
80	Divergence detected	0.449	0.45	0.458	Divergence detected
90	0.127	0.444	0.448	0.451	0.113
100	0.118	0.428	0.431	0.433	0.11
110	0.412	0.415	0.412	0.421	0.1
120	0.104	0.301	0.399	0.397	0.1
130	0.1	0.362	0.385	0.395	0.1
140	0.095	0.347	0.379	Divergence detected	0.095
150	Divergence detected	Divergence detected	0.378	0.379	0.089
160	0.089	0.347	0.345	0.354	0.085
170	0.086	0.318	0.364	Divergence detected	Divergence detected
180	0.083	0.301	0.327	0.327	Divergence detected

Case 5

Velocity	Biogas-air	Methane- air	Propane- air	Octane- air	Hydrogen-air
40	0.51	0.565	0.51	0.478	0.62
50	0.452	0.505	0.454	0.455	0.55
60	0.415	0.467	0.417	0.418	0.53
70	0.387	0.442	0.512	0.392	0.5
80	0.367	0.421	0.368	0.369	0.47
90	0.35	0.405	0.352	0.352	0.46
100	0.337	0.389	0.338	0.338	0.45
110	0.324	0.379	0.326	0.326	0.43
120	0.31	0.368	0.358	0.312	0.42
130	0.304	0.36	0.301	0.301	0.41
140	0.29	0.355	0.289	0.289	0.4
150	0.289	0.348	0.29	0.29	0.419
160	0.281	0.343	0.281	0.282	0.405
170	0.277	0.338	0.278	0.281	0.399
180	0.267	0.334	0.268	0.269	0.398

Appendix B

Biogas Composition

The composition of biogas-air used in the study is illustrated below

Species	Mole Fraction
CH_4	0.08620
CO_2	0.05747
H_2O	0.17878
N_2	0.6722
H_2S	0.00535

References

[1] Kailasanath, K., “Recent Developments in the Research on Pulse Detonation Engines," AIAA Journal, Vol. 41,No. 2, 2003, pp. 145-159.

[2] Roy, G.D., Frolov, S.M., Borisov, A.A., and Netzer, D.W., “Pulse Detonation Propulsion: Challenges, Current Status, and Future Perspective," Progress in Energy and Combustion Science, Vol. 30, No. 6, 2004, pp. 545-672.

[3] Lu, F.K., “Prospects for Detonation Propulsion," invited lecture, 9th International Symposium on Experimental and Computational Aerothermodynamics of Internal Flows, September 811, 2009, GyeongJu, Korea, 2010.

[4] Frolov, S.M., “Liquid-Fueled, Air-Breathing Pulse Detonation Engine Demonstrator: Operation Principles and Performance," Journal of Propulsion and Power, Vol. 22, No. 6, 2006, pp. 1162-1169.

[5] Lee, J.H.S., The Detonation Phenomenon, Cambridge, New York, 2008.

[6] Coleman, M.L., Overview of Pulse Detonation Propulsion Technology, Chemical Propulsion Information Agency, 2001, CPTR 70

[7] Jinnala, V.V.S., “Transient Flow Analysis of Filling in Pulse Detonation Engine,” Master's Thesis, Department of Mechanical and Aerospace Engineering, The University of Texas at Arlington, Arlington, TX, 2009.

[8] Chan, W.M., Gomez, R.J., III, Rogers, S.E., Buning, P.G., “Best Practices in Overset Grid Generation,” AIAA Paper 2002–3191, 2002.

[9] Pointwise V17.2R1 Training notes, 2014.

[10] “Creating a Butterfly O-H Topology for Structured Grids”, http://www.pointwise.com/DIY/Butterfly-Topology.shtml, accessed April 23, 2015.

[11] Ansys Fluent Theory Guide, 2009

[12] Václav D, Václav Ž, Pavel Z.,“Simulations of Two-Phase Flow In FLUENT”, Bakker A., Applied Computational Fluid Dynamics, Lecture 5-Solution Methods, Fluent Inc., 2002.

[13] Gridgen Tutorials, Chapter 6., “Intersecting Pipes: Pole Grid Construction (Top Down)”, 2003.

[14] Rongrat W.,“Numerical Study of Sidewall Filling for Gas-Fed Pulse Detonation Engines,” MSAE thesis, Department of Mechanical and Aerospace Engineering, University of Texas at Arlington, 2012.

[15] Stenmark, E., “On Multiphase Flow Models in ANSYS CFD Software,” Master’s Thesis in Applied Mechanics, Chalmers University Of Technology, 2013.

[16] Wahid, M.A., Alhamid, I., Pamitran, A. and Sheriff, J.M., “Feasibility Study of Pulse Detonation Engine Fueled by Biogas, Applied Mechanics and Materials (Volume 388), 257-261, August 2013.

[17] Best Practices for Filling Applications Using VOF, FLUENT user manual.

[18] Anderson, J.D., Jr. “Computational Fluid Dynamics: The Basics with Applications”, McGraw Hill, 1995.

Biographical Information

Swati Chandran was born and raised in Mumbai, India. She did her undergraduate work at the Institute of Aeronautical Engineering, Hyderabad, India. She received her Bachelors' of technology in Aeronautics in 2013. She began work on her Masters' of Science in Aerospace Engineering in Fall 2013 at the University of Texas at Arlington, Arlington, Texas.